Optimization study of the adsorption of malachite green removal by MgO nano-composite, nano-bentonite and fungal immobilization on active carbon using response surface methodology and kinetic study

Mohammed Taha Moustafa Hussien Hamad[1*]

Abstract

Malachite green a typical organic dye containing triarylmethane, is discharged in wastewater by textile and leather manufacturing plants. MG can pollute the environment, and it represents a major hazard to humans and various living organisms. We have thus worked toward developing the optimum dye-absorptive material, which should possess the following characteristics: excellent adsorption capacity, good selectivity, favorable recycling and reuse potential, and ease and quickness of adsorption. In this study, nano-bentonite, novel hybrid MgO-impregnated clay, and fungal composites were synthesized for Malachite green removal from aqueous solution. Response surface methodology (RSM) was used for the optimization of the synthesis of adsorbents to achieve simultaneous maximum malachite green removal. The composites were characterized by Fourier transform infrared spectroscopy (FTIR), scanning electron microscopy (SEM) and X-ray diffraction (XRD). According to the obtained results, MgO-impregnated clay exhibits a exhibited a higher adsorption capacity of MG than nano-bentonite and pure bentonite. The malachite green adsorption isotherm on MgO-impregnated clay corresponded with the Freundlich isotherm. However, the Langmuir adsorption isotherm was a superior fit for nano-bentonite. The adsorption activities of nano-bentonite and MgO-impregnated clay were fitted into a pseudo-second-order kinetic model. Based on the root-mean-square error, bias, and accuracy, statistical research has shown that the Halden model has optimal accuracy. In addition, despite being recycled numerous times, the adsorbent maintained its high structural stability and removal effectiveness for nano-bentonite (94.5–86%) and MgO-impregnated clay (92–83%).

Keywords Malachite green, Response surface methodology, Nano-bentonite, MgO-impregnated clay adsorbent

Introduction

The global economy's growths due to industrialization, accompanied by urbanization high rate, have led to severe anthropogenic pollution impacting both the environment and human health [1]. Globally, about 280,000 tons of synthetic dyes are discharged into natural streams every year from wastewater produced by a variety industries, such as leather, food, textile, paper, cosmetic, printing, and carpet manufacturers [2]. The textile industry consumes 100–200 L of water per kg of textiles produced,

*Correspondence:
Mohammed Taha Moustafa Hussien Hamad
Mohamed_taha@nwrc.gov.eg
[1] Central Laboratory for Environmental Quality Monitoring, National Water Research Center, Shubra El Kheima 1 6210001, Al Qalyubia Governorate, Egypt

resulting in the generation of large amounts of wastewater during the dyeing process [3]. Malachite green (MG) is a synthetic dye used to dye silk, cotton, leather, wool, and paper, and it is also employed as a fungicide and disinfectant in the fish farming industry, as it affords the control of fish parasites and diseases [4]. MG is a cationic triphenylmethane compound that is highly soluble in water [5]. It is also highly toxic to mammalian cells at concentrations below 0.1 g/mL [6]. Malachite green is characterized by a complex molecular structure, high stability, non-biodegradability, and high resistance to light and oxidizing agents. The Malachite green discharge has an adverse impact on the visual quality of water bodies, and it interferes with the life cycles of aquatic organisms by reducing the penetration of sunlight into the water, which inhibits photosynthesis and plant growth, thereby affecting the biological activity of aquatic animals by interfering with the physiology of the pituitary liver, gills, kidneys, intestines, gonads, and gonad vegetative cells; moreover, the synthetic dyes present in water bodies also cause soil contamination [5, 7, 8]. MG is hazardous to humans, and mutagenic; in addition, its presence affects the immunological and reproductive systems [9]. MG inhalation can cause inflammation of the respiratory tract, while its swallowing can cause inflammation of the digestive tract [10]. The dye can be converted into leucomalachite green and carbinol, which is toxic to humans. In fish muscles, fat, and internal organs, MG has a half-life of 10 days [11]. This cationic dye is also durable in the environment, with a half-life of 12.9–50.34 days in sediment [12]. Many technologies have been used to treat textile wastewater, including physical, chemical, and advanced treatment methods, such as membrane filtration, ion exchange, electrochemical technology, coagulation, flocculation, reverse osmosis, chemical oxidation, ozonation [13], and biological treatment for fungi and bacteria effects [14]. However, most of these technologies have various disadvantages, including low efficiency, large capital investment, high energy consumption, high cost, non-selectiveness, unsuitability for large-scale applications, and the formation of harmful secondary sludge [15]. Among the treatment strategies, adsorption is one of the most appealing and efficient methods for removing dyes from polluted water samples. Recently, scientists have developed an efficient and economical adsorbent material, nano-clay polymer composites, to overcome the shortcomings of traditional purification methods for textile industry wastewater and reduce their environmental threat. This technique provides various advantages, including a simple design, recyclable adsorbents, simple operation, nontoxicity, low cost, and a modest initial investment [16]. These recyclable adsorbents include activated carbon (AC) [17], lime peel [18], natural clay

[19], hematite iron oxide nanoparticle [20] and pumice [21]. In recent years, researchers have shown an increasing interest in metal oxides, specifically magnesium oxide nanoparticles (nMgO), due to their beneficial characteristics, such as high specific surface area, low density, nontoxicity, affordable production, and superior physical properties. According to a study by Elkhatib et al. [22], mesoporous MgO nano-sheets exhibited the maximum adsorption capacity of 200 mg/g for Cd(II) removal from industrial wastewater. Bentonite, a type of clay mineral that contains mainly montmorillonite, has also gained popularity in various industries due to its abundance in nature, low cost, large surface area, good chemical and mechanical stability, and its ability to exchange cations with those found in aqueous solutions of organic or inorganic salts, as reported by Aichour and Zaghouane [23]. Raw bentonite typically has a low adsorption capacity for cationic dyes, so it is often modified through physical or chemical treatments to increase its absorption power. Chemically treated bentonite has been used to remove cationic basic methylene blue [24], metal ions [25], and crystal violet [26]. Nano-clays such as nano-bentonite have become increasingly popular in recent years as a highly effective tool for the removal of pesticides. Studies conducted by El-Nagar et al. [27] have demonstrated that nano-bentonite has the highest removal capacity among the known clays. Natural clay usually has high cation exchange capacity and has been used to adsorb dyes. Mechanisms in the adsorption of malachite green on clay, such as the existence of dipolar interactions between the negative charge of the carboxylate group and MG as a cationic dye, the H-bonding interaction, and the dipole–dipole H-bonding interaction [28]. Malachite green adsorption was studied by Dehbi et al. [20] using hematite iron oxide nanoparticles; for MG, the percentage of removal reached 94%. Response surface methodology (RSM) is a mathematical and statistical tool used to analyze the effects of independent variables on a process under consideration to predict the target response and can provide accurate results with fewer experiments than classical methods [29]. Box–Behnken design (BBD) and central composite design (CCD) are two of the most popular and efficient RSM methods that have been successfully used in studies for dye removal, such as removal of malachite green from water by immobilization of Burkholderia cepacia [30], sorption of crystal violet and methylene blue onto water hyacinth (Rajnikant Prasad et al. 2016), removal of remazol black B by *Caulerpa scalpelliformis* [31]. We hypothesize that the modification of bentonite surface by coating with Mg oxides nanoparticles could significantly enhance its reactivity and adsorption affinity for MG. This could open up new avenues for the efficient removal of dyes from waste streams. Thus,

this study aims to evaluate the advantages of each single component and achieving superior sorption efficiency of malachite green dye. Furthermore, the proposed fabrication method is clean, chemical free, cost-effective and time-saving and eco-friendly. The fabricated nano-bentonite, MgO-impregnated clay, and immobilized *Mucor* sp. on active carbon composite are mainly made from natural sources which are safe to human and environment. These developed adsorbents composite were sufficiently characterized by XRD, TEM, SEM/EDX, and FTIR techniques. Various factors affecting the adsorption of malachite green dye were optimized by response surface methodology. The suitable isotherm and kinetic models were predicted for the adsorption process. The reusability and regeneration of the developed adsorbents were clearly investigated for multiple cycles.

Materials and methods
Chemicals and materials
The bentonite used in this study was obtained from CMB Co. (Egypt). Magnesium chloride dihydrate ($MgCl_2 \cdot 2H_2O$) and hydrochloric acid were provided by Sigma-Aldrich Co. (Egypt).

Analytical measurements for nano-bentonite, raw bentonite and MgO-impregnated clay characterization
Raw bentonite, nano-bentonite and MgO-impregnated clay were characterized by Transmission electron microscopy (TEM) with a JEOL-JEM-2100.

Fourier transform infrared spectroscopy
FTIR spectra of the adsorbents were captured using Bruker-VERTEX 80 V in 4000–400 cm^{-1} range for evaluating the surface functional groups of the adsorbents.

X-ray diffraction (XRD)
X-ray diffraction (XRD) of raw bentonite, nano-bentonite and MgO-impregnated clay were analyzed using PANalytical X'Pert Pro (United Kingdom) with operating current at 30 mA and the voltage at 40 kV. The pattern was recorded by CuKα radiation [32].

Scanning electron microscope (SEM)
The Scanning electron microscope (SEM) can help in the determination of morphology of raw bentonite, nano-bentonite and MgO-impregnated clay. (SEM) scanning electron microscope images were obtained by a Brand FIE Quanta 250 device of a spectroscopy X-ray (EDX).

Preparation of the MG dye solution
The cationic dye MG (Fig. 1; chemical formula: $C_{46}H_{50}N_{42}C_2HO_4C_2H_2O_4$, MW: 927.1 g/mol) was purchased from MERCK Pvt. Ltd (England). A 1 g sample
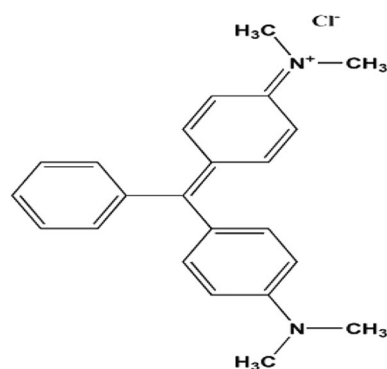

Fig. 1 Structural formula of Malachite Green

of the appropriate MG was dissolved in 1000 mL of distilled water to produce an MG stock solution of 1000 mg/L concentration. The stock solution was then used to prepare MG solutions of concentrations ranging from 30 to 150 mg/L. The initial pH of the stock solution was adjusted by adding to it 0.1 M HCl or NaOH. A 50 mL aliquot of the MG stock solution was used for each of the experiments. All experiments were conducted in triplicate.

Fabrication of nano-bentonite
An amount of 21.2 g of bentonite powder and 100 mL of 12 M HCl solution were combined, and the resulting mixture was heated in a magnetic stirrer at around 343 K and stirred at a rate of 340 rpm for 120 min. Subsequently, the obtained suspension was filtered and the precipitate was repeatedly washed with distilled water until the pH of the water used to wash the residue reached neutrality. The thus obtained acid-activated bentonite was dried in the oven for 5 h at a temperature of 373 K. The precipitate was then ground in a mortar to produce a powder, which was calcined in a furnace at 600 °C for 2 h [33].

Preparation of MgO-impregnated clay nanocomposites
A mixture of 7.1 g of bentonite clay and 100 mL of 1.25 M magnesium chloride solution was stirred for 6 h. After stirring; the solution was poured into a glass petri dish and dried in an oven at 150 °C. The dried mixture was crushed to a fine powder and calcined in a muffle furnace at 450 °C for 2 h. The homoionic bentonite was dialyzed in deionized water until it was free of chloride. Then, it was separated by centrifugation [32, 34]. The calcined powder was cooled, washed twice with deionized water, and dried at 70 °C for 6 h [35].

Determination of the zero point charge of the adsorbent

The pH point of zero surface charge characteristics of nano-bentonite, raw bentonite and MgO-impregnated clay was determined using the following method [36]: 50 mL of 0.1 M NaCl solution was transferred into 100 mL Erlenmeyer flasks, with the initial pH (pHi) values adjusted from 3.0 to 12.0 by adding 0.1 M HCl or NaOH. Next, 0.3 g nano-bentonite, raw bentonite and MgO-impregnated clay were added to each flask, and the suspensions were stirred continuously for 24 h. The final pH values of the supernatant liquids were assessed after 24 h. The pH $_{PZC}$ was plotted against the difference between the initial and final pH (pHf) values. The zero point of charge (pH$_{ZPC}$) of the substance was considered the point, where the resulting curve intersected the pHi axis at pH$= 0$.

Batch adsorption experiments

Batch adsorption experiments were carried out to achieve the optimum operating conditions for removing of the MG dye. 100 mL solution of dye initial concentration was taken in 250 mL flasks and a known amount of raw bentonite, nano-bentonite and MgO-impregnated clay, the adsorbents were added to the solutions. The mixture was shaken mechanically at a constant speed of 200 rpm using rotary shaker (Dragon LAB, skp-0330-pro-Germany). The effects that different experimental parameters had on the efficiency of MG removal were investigated. In particular, various values were utilized for the pH (3.0, 5.0, 6.0, 7.0, 8.0, 9.0, 10.0, and 11.0), contact time (10–60 min), adsorbent dosage (0.05, 0.1, 0.2, 0.5, 0.7, and 1.2 g/L), initial dye concentration (50–250 mg/L), and temperature (298, 303, 323, and 343 K). The initial pH values were adjusted using 0.1 M HCl or 0.1 M NaOH solutions and a pH meter (Multi 9620 IDS-pH meter, WTW, Germany). Each experiment was performed three times and the averages values of the measurable were calculated and presented. Samples were taken out after the equilibrium time (60 min) and centrifuged at 4000 rpm for 25 min to completely separate the raw bentonite, nano-bentonite and MgO-impregnated clay from the solution and MG concentrations in the supernatants were determined measuring the supernatants' absorption at the wavelength at which MG exhibits its maximum absorption ($\lambda_{max} = 620$ nm) using a spectrophotometer (Thermo Fisher Scientific, Orion Aquamat 8000, USA). MG removal efficiency, R (%), was determined through the following equation:

$$\%R = \frac{C_o - C_f}{C_0} \times 100 \tag{1}$$

where C_0 and C_f represent the initial and final concentrations of the dye solution (mg/L).

The adsorption capacity (q_e, mg/g) at equilibrium, was determined using the following equation:

$$q_e = \frac{(C_i - C_e)}{M} V \tag{2}$$

where C_i (mg/L) and C_e (mg/L) are the MG dye concentrations in the initial solution and at equilibrium, respectively; V (L) is the volume of the solution; and w is the mass of the adsorbent (mg).

Equilibrium studies

In the current investigation, the equilibrium condition for the adsorption of MG on raw bentonite, nano-bentonite and MgO-impregnated clay was described using the Langmuir, Freundlich, and Tempkin models, as given by Fabryanty [37].

Kinetic studies

Pseudo-first-order and pseudo-second-order kinetic models were utilized to analyze the kinetics of MG adsorption on the adsorbents. The pseudo-primary-order model, in its linear form is described by Kowanga et al. [38].

Experimental design using the response surface methodology

As a design method, the response surface methodology (RSM) is a mathematical tool that uses a second-order equation to determine the best conditions between the controllable input factors and the response variable. The effects of various factors, such as pH ($X1$), temperature ($X2$), adsorbent dosage ($X3$), and initial concentration ($X4$), on the decolorization process, were studied using the Box–Behnken design. The equation $N = 2 K(K^{-1}) + C$ is used to determine the number of experiments required for a Box–Behnken design (BBD). In this equation, N represents the frequency of samples; K indicates the frequency of variables, and C shows the frequency of central points [39]. Calculations suggested a total of 29 experiments. Twenty-nine experimental runs were obtained according to the three levels of each variable; low level (-1), level; (0) (medium) and high level (1) were used to design and analyze the experiments. The second-order quadratic equation model was assessed to predict the optimum value between the dependent and independent factors. The correlation's general form can be stated according to the following equation:

$$Y = \beta_o + \sum_{i=1}^{n} \beta_i X_i + \sum_{i=1}^{n} \beta_{ii} X_i^2 + \sum_{i=1}^{n-1} \sum_{j=1+1}^{n} B_{ij} X_i X_j \tag{3}$$

Here, Y is the predicted response factor (the removal of MG), and X is the input variable. β_0, β_j, β_{jj}, and β_{ij} are the intercept, linear effect, square effect, and interaction effect, respectively. N is the quantity of input-controlling coded variable. The coefficient of determination (R^2) and Fisher's F-test were used to describe the quality of the quadratic model equation. Using Design-Expert 13, an analysis of variance (ANOVA) was conducted to determine the model's statistical significance.

Microbial toxicity

The microbial toxicity of the Malachite green dye on *Escherichia coli*, *Staphylococcus aureus*, and *Pseudomonas aeruginose* was investigated. Furthermore, using an agar well assay, the toxicity of the dye and its breakdown products were investigated. After 24 h of incubation at 37 °C, the zone of microbial growth inhibition was recorded.

Isolation and identification of malachite green

A pure fungal strain was isolated from wastewater, and seven fungal strains capable of decolorizing the malachite green dye were identified. The ability of the fungal strain to decolorize the dye was carried out in Sabouraud's Dextrose Broth (SDB) amended with malachite green dye (5 mg L^{-1}). The Erlenmeyer flasks contained 100 mL sterile media with dye and were inoculated with an immobilized fungal strain. The flasks were placed in an incubator shaker for 72 h at 30 ± 2 °C. The samples were withdrawn aseptically at 24, 30, 36, 48, and 72 h alternately and centrifuged at 4500 rpm for 10 min. Furthermore, the supernatant was scanned in a spectrophotometer at $\lambda_{\max}$ (620 nm) of malachite green dye. The control flasks underwent similar former conditions, but without fungal biomass. Among the isolated strains, *Mucor* sp. optimally decolorized malachite green, with a removal efficiency of

92.2%. The resultant sequence was given to the National Center for Biotechnology Information (NCBI), where it was assigned an accession number (ON934589.1). Figure 2 shows that the gene sequence was examined using NCBI's Basic Local Alignment Search Tool (BLAST) and that a phylogenetic tree was formed using Mega 7.0.

Immobilization of Mucor sp. in alginate

A sodium alginate stock solution prepared using 2 g of sodium alginate (R&M Chemicals) was dissolved in 50 mL of distilled water. Separately, bentonite was made by dissolving 1.1 g of bentonite and 1.2 g of active carbon in 50 mL of distilled water and stirring the mixture to create a homogeneous suspension. Afterward, the bentonite solution and alginate were combined and autoclaved for 20 min at 121 °C. A total of 10.8 g pellets of fungal cells were obtained through centrifugation (46,000 rpm for 21 min) after they were cultured in sabroud dextrose broth. They were then combined with alginate (2% by weight) and bentonite (1% by weight) and dropped separately into 100 mL of CaCl$_2$ solution (3% by weight) with continuous stirring. The beads formed were left for 1 h at 37 °C, washed thoroughly in distilled water, and stored for 24 h at 4 °C.

Optimization of MG decolorization using Box–Behnken design

The Box–Behnken design was used to examine the effects of four significant variables on the decolorization of MG by immobilized *Mucor* sp. These variables included pH (5–9) (A), temperature (25 °C–45 °C) (B), fungal concentration (1.0, 2.0, and 3.0 g), contact time (24–72 h) (C), and initial concentrations (5–200 mg/L) (D). Flasks were kept in an incubator shaker at 120 rpm, and the optical density at $\lambda_{\max}$ (620 nm) was recorded to determine the concentration of MG in the supernatant.

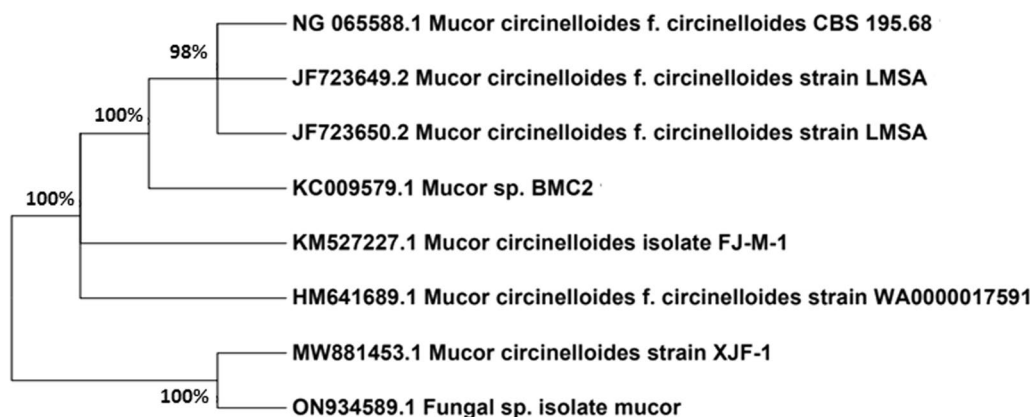**Fig. 2** Phylogenetic tree of the fungal isolate *Mucor* sp.

Model verification using the experimental data

Data were analyzed using a variety of statistical techniques, including the root mean square error (RMSE), which was calculated according to Eq. (4), where n and p are the number of experimental data and parameters number of the model, respectively. Where Pdi and Obi are predicted values and experimental data, respectively. The models for describing the maximum growth rate of *Mucor* sp. were evaluated using both the bias factor (Bf) and the accuracy factor (Af), as calculated according to Eqs. (5) and (6). A model is considered fail-safe if its *Bf* value is more than 1.0 and fail-dangerous if its *Bf* value is less than 1.0. On the other hand, the value of Af is never larger than 1.0, with accurate models being characterized by values for this parameter that are close to 1.0. The Akaike information criterion (AIC) is a measure of the relative quality of mathematical analyses for a given set of data, and a criterion for error prediction was calculated according to Eq. (7). The R^2 formula is modified for nonlinear models to incorporate the residual mean squared error and S^2y, which is the total variance of the *Y*-variable [40].

$$\text{RMSE} = \sqrt{\sum_{i-1}^{n}\left(\frac{\text{experimental/predicted}}{n-p}\right)2} \qquad (4)$$

$$\text{Bf} = 10 \exp\left[\ln 10\left[\sum \log\left(\left(\text{experimental/predicted}\right)/n\right)\right]\right] \qquad (5)$$

$$\text{Af} = 10 \exp\left[\ln 10\left[\sum\left|\log\left(\left(\frac{\text{experimental/predicted}}{n}\right)\right)\right|\right]\right] \qquad (6)$$

$$\text{AICc} = 2p + n \ln\left(\frac{\text{RSS}}{n}\right) + 2(p+1) + \frac{2(p+1)(p+2)}{n-p-1} \qquad (7)$$

$$\text{Adjusted}\left(R^2\right) = 1 - \frac{\text{RMS}}{S^2y} \qquad (8)$$

$$\text{Adjusted}\left(R^2\right) = 1 - \frac{(1-R2)(n-1)}{(n-p-1)}. \qquad (9)$$

Results and discussion

Characterization of nano-bentonite, raw bentonite and MgO-impregnated clay

X-ray diffraction (XRD)

An XRD analysis (Fig. 3a) was conducted to determine the mineralogical constitution and crystalline nature of the raw bentonite sample. The intensities of the XRD peaks were relatively high, which is an indication of high crystallinity. Based on the XRD pattern, we
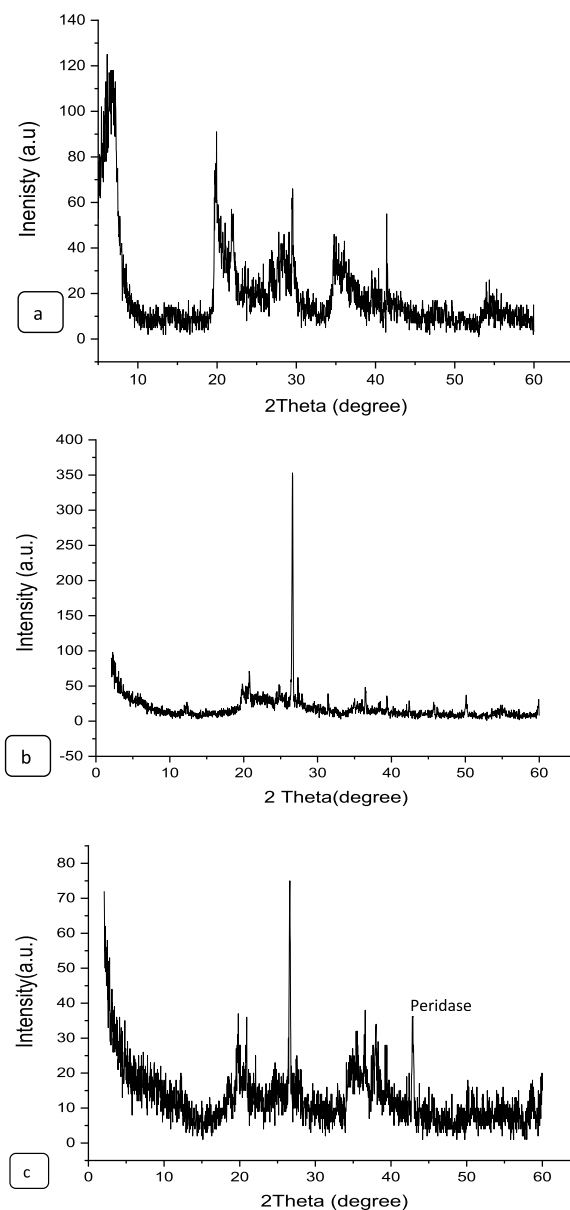

Fig. 3 X-ray diffraction patterns of **a** raw bentonite, **b** nano-bentonite and **c** MgO impregnated clay

can conclude that montmorillonite and quartz were the major constituents of raw bentonite, a conclusion confirmed by standard data for bentonite (ref's: 01-058-2010 and 00-075-4411). The dominant diffraction peaks for raw bentonite were found at values for Bragg's angle (2θ) of $\sim$19.7°, 21.95°, 50.88°, 34.79°, and 53.75 which are due to the presence of quartz, and $\sim$26.81°, 29.3°, 41.38 and 53.75°, which are due to the presence of montmorillonite. An XRD analysis (Fig. 3b) was conducted to determine the mineralogical constitution and crystalline nature of the nano-bentonite sample. The intensities of

the XRD peaks were relatively high, which is an indication of high crystallinity. Based on the XRD pattern, we can conclude that Kaolinite-1A and quartz were the major constituents of modified bentonite, a conclusion confirmed by standard data for bentonite (ref's: 01-075-8320 and 00-058-2028). The dominant diffraction peaks for nano-bentonite were found at values for Bragg's angle (2θ) of ~ 12.2°, 20.79°, 26.60°, ~ 27.3°, 34.88°, and. 39.43°, which are due to the presence of kaolinite, and 19.79°, 36.47°, 42.4303°, 45.7659°, and 50.107°, which are due to the presence of quartz. The crystalline structure for pure bentonite and nano-bentonite with HCl addition is hexagonal [41]. The decrease of the interlayer space of nano-bentonite indicates that some molecules of MG were adsorbed on top of the layers, a phenomenon that may be due to an electrostatic interaction between the positively charged groups of dye surfactant molecules with the negatively charged surface sites of nano-bentonite [42, 43]. Scherrer's equation (10) has been used to calculate the crystallites' size (D):

$$D = \left(\frac{k\lambda}{\beta} \cos\theta \right) \tag{10}$$

where D is the crystallite size, β is the full width at half maximum, λ is the X-ray wavelength, and θ is Bragg's angle. The estimated size of the average nano-bentonite crystallite was ~ 38 nm. In Fig. 3c are reported the XRD patterns of MgO-impregnated clay. XRD pattern of MgO in the crystalline cubic phase. The sharpness and the intensity of peaks indicate the well-crystalline nature of the prepared sample According to this figure, the clay sample exhibited various peaks of different intensities. Indeed, peaks were observed at 2θ values of 20.91°, 26.61°, 36.57°, 37.63°, 50.14°, 56.72°, 12.27°, 18.60°, and 58.76°, indicating the presence in the sample of quartzite (40%), kaolinite (10%), and MgO nanoparticles (50%), respectively. The peak at 2θ diffraction angle of 42.83∘ (JCPDS: 75-0447) can be assigned to formation of pure phase of periclase MgO [35]. The average crystallite size was estimated to be ~ 46.6 nm.

FT-IR spectroscopy
The FTIR examination of bentonite clay revealed an intense band at 990 cm^{-1}, which is attributed to the silicate (Si–O–Si) structure, as well as additional other bands at 914 cm^{-1} shows the stretching vibration of Al–Al–OH and Al–Fe–OH bonds in the octahedral sheet of the bentonite structure. The band at 794 cm^{-1} is attributed to quartz in the raw bentonite (Fig. 4a). The band at 712.44 cm^{-1} corresponds to the bending vibration of the Al–O bonds in the octahedral sheet of the bentonite structure. The stretching vibration band at 642 cm^{-1} is ascribed to the deformation
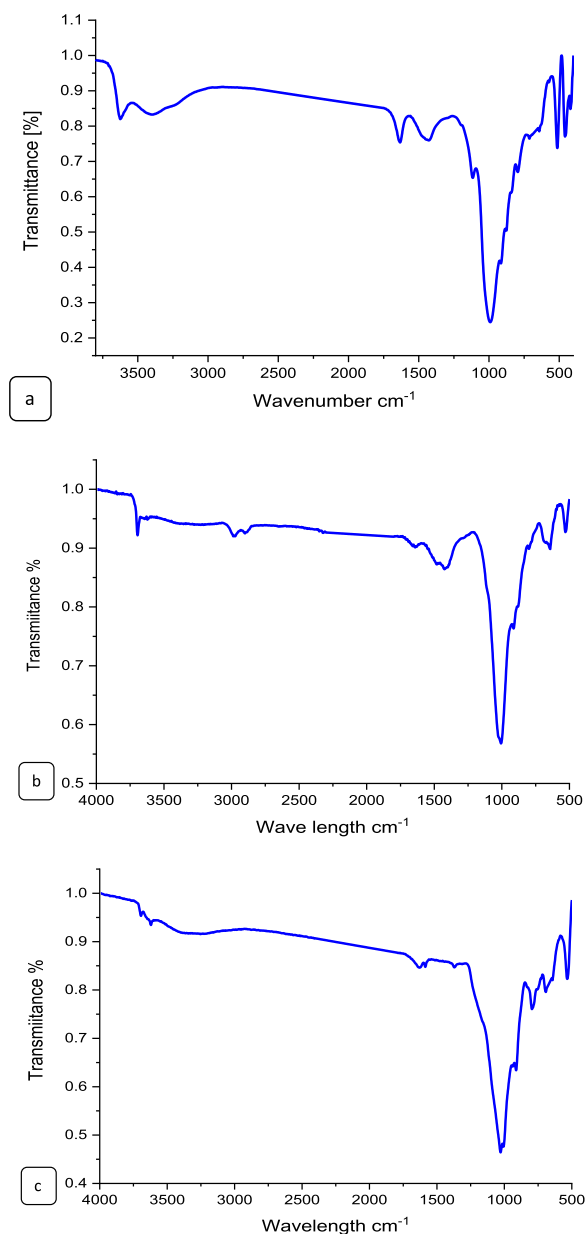

Fig. 4 FTIR images of **a** raw bentonite, **b** nano-bentonite and **c** MgO impregnated into clay

and bending modes of the Si–O bond. The bands at 458 and 513 cm^{-1} are attributed to (Al–O–Fe) and (Al–O–Si) bending vibrations, respectively [32]. Abdelnaby et al. [44] found that bond O–H deformation of the contained water molecules in the silicate matrix is related to the small band at 1633 cm^{-1}. The band at 1428.18 cm^{-1} corresponds to the bending vibration of the Al–OH and Si–OH bonds in the octahedral and tetrahedral sheets of the bentonite structure. The absorption bands between 3392.58 cm^{-1} could be ascribed

to stretching vibrations of structural OH-stretching vibrations that have Al and Mg coordination groups with octahedral layer of montmorillonite and water [45]. The broad infrared spectroscopy bond-stretching peak between 3693.93 and 1630.21 cm^{-1} wave numbers (Fig. 4b is indicative of the presence of OH stretching in hydration water on the nano-bentonite surface. Notably, in [46] detected peaks on the nano-bentonite surface at 3450 and 1650 cm^{-1} wave numbers, which confirmed the existence of OH groups. In the FTIR spectra recorded in the present study. The stretching vibration of the Si–O bond was detected as a very strong absorption band at 1006 cm^{-1}, providing strong evidence of the presence of a silicate structure. Due to the electrostatic attraction between the bentonite Si–O groups and the MG's positively charged moiety, and it indicates that the Si–O groups of nano-bentonite may be involved in the process of dye adsorption, while the shift in the wave number values of the peaks indicates that substrate adsorption did indeed occur [47]. The peaks at 920.80 cm^{-1} could be attributed to the bending vibration of Al–OH–Al groups and Al–O and Si–O vibration, respectively [48]. The presence of quartz in nano-bentonite may be inferred from the peaks at 795 cm^{-1} and 533 cm^{-1}. According to Zhirong et al. [49], the presence of quartz is confirmed by a band appearing at 796 cm^{-1}. Tastan et al. [50] attribute the bands at 500–400 cm^{-1} wave numbers to the bending vibrations of the Al–O–Si (octahedral Al) and Si–O–Si (tetrahedral Si) groups. The FTIR spectrum of the species obtained after MgO-impregnated clay underwent MG adsorption is reported in Fig. 4c. The bands at 3861 and 3622 cm^{-1} correspond to the stretching vibrations of the O–H bond of Si–OH groups coordinated to two Al atoms, whereas the band at 3207 cm^{-1} is due to MG captured by MgONPs. The band at 1641 cm^{-1} is due to the bending of water molecules, and the peak at 1423 cm^{-1} is attributed to the Si–O bond vibration mode. The deep band at around 1040 cm^{-1} is due to the stretching of the Si–O bond in the Si–O–Si groups of the tetrahedral sheet. The peak at 913 cm^{-1} is due to the deformation of the Al–Al–OH group; indeed, this peak is very close in position to the peaks at 913 and 914 cm^{-1} reported by Popli and Patel [51]. The FTIR peaks appearing at 800 cm^{-1} and 620 cm^{-1} were assigned to the stretching vibration of Mg–OH and Si–O–Mg, respectively, indicating the presence of MgO-impregnated bentonite. The peak at 643 cm^{-1} was attributed to the stretching vibration of Mg–OH, confirming that MgO was present in the bentonite, while the peak at 537 cm^{-1} is associated with the bending vibration of the Al–O–Si group, and their observation is indicative of the presence of crystalline quartz.

Morphological structure of prepared adsorbents

As can be evinced from Fig. 5a, b, the TEM images of nano-bentonite and MgO-impregnated clay indicated that these samples were irregularly shaped, heterogeneous, and semi-spherical. The surface morphologies of raw bentonite, nano-bentonite and MgO-impregnated clay were investigated by SEM (see Fig. 5. The surface of raw bentonite has a porous structure which increases the contact area and promotes adsorption at active sites of the positively charged ions [44]. It is evident that bentonite clay particles were made up of heterogeneous aggregates of assorted sizes and shapes. These grains form a stack of sheets, indicating clay layers. A little bright crystallite settles on the sample's surface, which could be made of free silica [52]. The elemental compositions of raw bentonite has been studied by EDX. The elemental composition of bentonite clay, nano-bentonite and nano-MgO-impregnated clay are shown in Fig. 5c and Table 1, which reveal that the dominant elements were O, Si, and Al in a percentage of 51%, 25.6%, and 7.04%, respectively, confirming the aluminosilicate structure. Na, Mg, K, Ca, and Fe are other exchangeable cations that exist in lower amounts [44]. Nano-bentonite was observed to have a smooth surface and an irregular shape, while surface morphology reveals a spongy appearance with an uneven structure. In addition, micrographs of the MgO-impregnated clay powder indicate the presence of huge agglomerates of extremely fine MgO particles, these data also suggest that the powder is highly porous. The generation of pores and voids may be caused by the bentonite clay swelling upon treatment with magnesium salt, which, upon desiccation and calcination, results in the formation of MgO clusters in the interlayer spaces of bentonite. At various magnifications, secondary electron images were acquired to study their morphologies and elemental compositions. The SEM image of the nano-bentonite and MgO-impregnated clay after adsorption of MG dye shows that the surface of the adsorbent is rough with an increased number of voids, as shown in Fig. 5e, f, respectively. Figure 5g displays the surface morphologies of the fungus hyphae and active carbon after they have absorbed the MG. The outer surface of the fungal biomass and active carbon (AC) are coated with particles with diameters ranging from 0.1 to 1 mm, suggesting that the dyes were primarily adsorbable onto the fungus hyphae and AC. The presence of polysaccharides in the fungal biomass cell wall gives the hyphae ball a great capacity for biosorption [12]. The average crystallite sizes of MgO-impregnated clay and nano-bentonite, which were estimated via the Debye–Scherrer equation, were 46.6 and 38.9 nm, respectively.
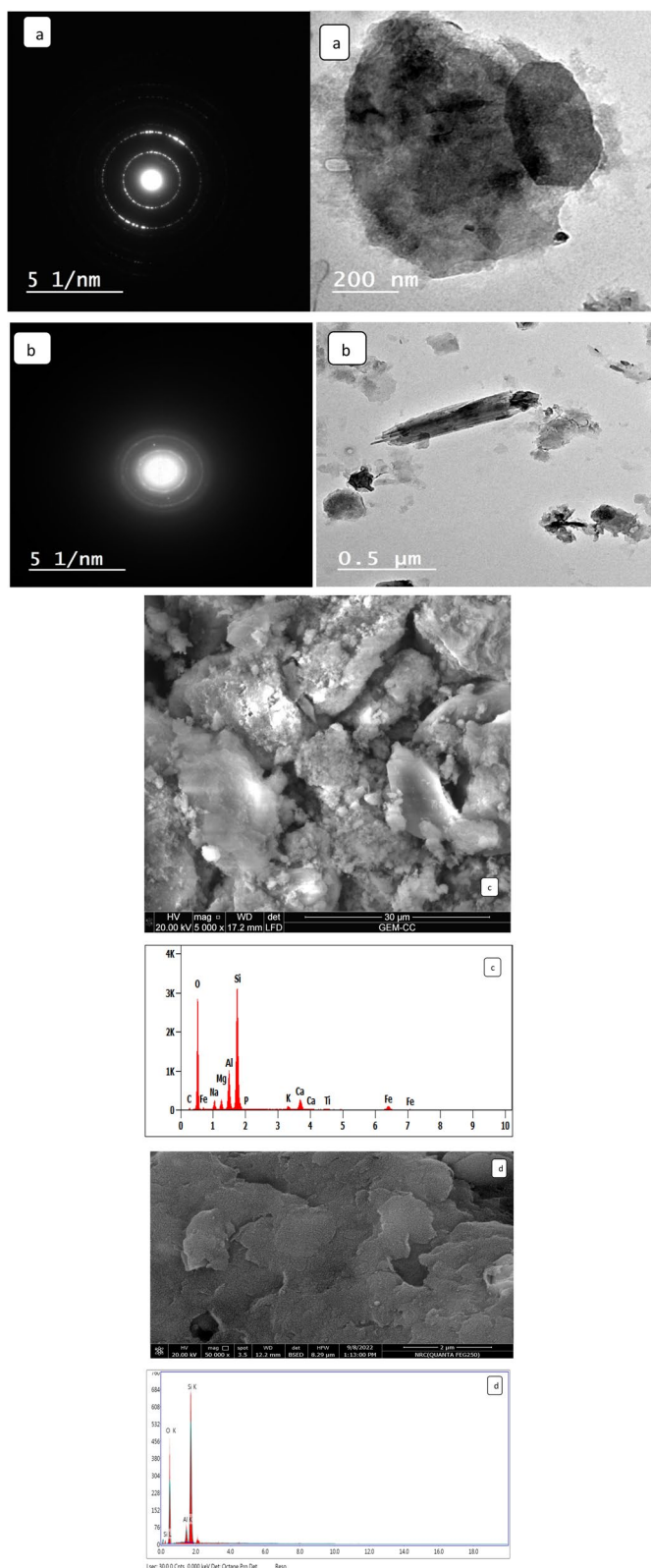
Fig. 5 TEM **a** nano-bentonite, **b** MgO impregnated clay, and SEM images and Energy dispersive X-ray analysis, **c** raw bentonite, **d** nano-bentonite within EDX, **e** MgO impregnated clay within EDX, **f** nano-bentonite after adsorption MG, **g** MgO impregnated clay after adsorption MG and **h** after adsorption MG by fungi low and high magnification, respectively
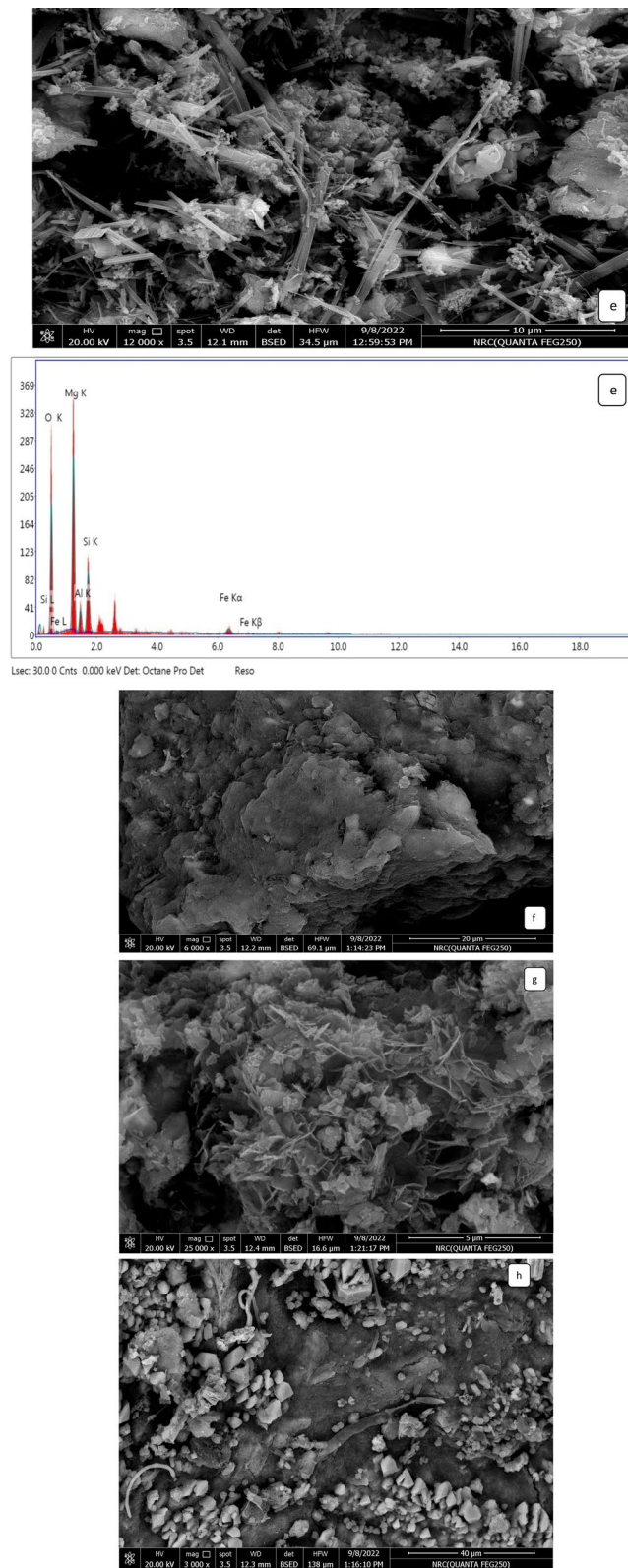
Fig. 5 continued

Table 1 DEX elemental analysis of raw bentonite, nano-bentonite and MgO-impregnated clay

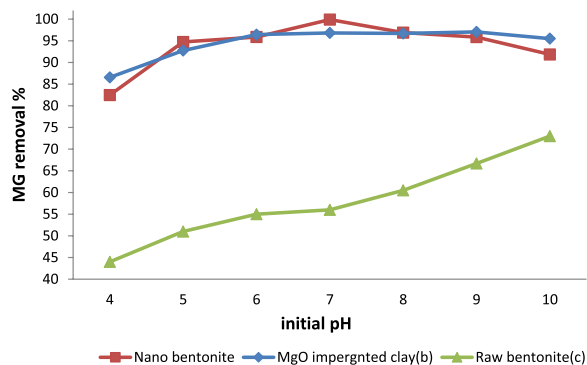| Adsorbent	Element	Weight%
Raw bentonite	C	1.94
	O	51.001
	Na	2.750
	Mg	1.837
	Al	7.074
	Si	25.644
	P	0.274
	K	1.160
	Ca	3.580
	Fe	4.153
Nano-bentonite	O	45.34
	Mg	31.94
	Al	5.53
	Si	12.94
	Fe	4.24
MgO-impregnated clay	O	55.6
	Al	4.36
	Si	40.03

Fig. 6 Effect of pH on MG dye removal by **a** nano-bentonite, **b** MgO impregnated clay and **c** raw bentonite

Influence of pH on MG adsorption

According to several studies, the initial pH of a solution is one of the most important environmental factors influencing the adsorption process, because it affects adsorbate solubility and surface charge, as well as adsorbate speciation and degree of ionization. The effect of the initial pH on the capacity of raw benonite, nano-bentonite and MgO-impregnated clay to adsorb MG was investigated over the 3.0–11.0 pH range. In Fig. 6 are reported data reflecting the influence that the initial pH had on dye removal, in conditions, whereby the initial concentration of the dye (50 mg/L), the contact time (60 min), the temperature (35 ℃), and adsorbent dosage (1.0 g) were kept constant. As can be evinced from Fig. 6, MgO-impregnated clay exhibited good adsorption, with the maximum percent removal of MG (97.04%) observed at pH 9.0. On the other hand, the maximum uptake of MG by nano-bentonite reached a value of 99.8% at pH 7.0. The maximum uptake of MG by raw bentonite reached a value of 73.2% at pH 10.0. The values for the zero point charge (pHzpc) of nano-bentonite, raw bentonite and MgO-impregnated clay were found to be 5.5, 6.1 and 7.1, respectively. The low adsorption capacity exhibited by the two adsorbents under < pHpzc conditions could be mainly attributed to the decrease in the number of negative charges on the adsorbents' surfaces and the increase in the number of positively charged sites in the adsorbents, which can cause electrostatic repulsion between the adsorbents and the dye molecules. As a consequence, the probability of MG molecules being adsorbed on the two adsorbents may decrease. By contrast, as the pH > pzc, the deprotonation of the sites on the surface of nano-bentonite and MgO-impregnated clay composites resulted in the number of negatively charged adsorbent sites to increase attracting the positive cationic MG, thus resulting in the observed increase in percentage removal of dye [53]. According to Messaoudi et al. [28] who examined the relationship between pH and the adsorption of MG Moroccan clay, and found in acidic media, the adsorption capacity of MG is low, this could be explained by the fact that the adsorbents are positive carrying the same charge of the cationic dye MG. This can be explained by the accumulation of OH^- ions on the surface of the adsorbent, which favors the adsorption of MG, which carries a positive charge on its surface, and, therefore, the appearance of the phenomenon of electrostatic attraction. In addition, more than pH > pHzpc, therefore, there is an increase in the negative charge density on the surface of the MG, which causes the elimination of MG. Similar conclusions were reached by Dehmani [19], who attributed the increase in adsorption observed as the pH 8 (94%) increased to a reduction in the competition for functional groups between the cations methylene blue and natural clay protons present in solution. Our findings paralleled those of Jinendra et al. [54], who discovered that the removal of MG dye by titanium coated graphite was lowest at pH 3.0 (56.2%) and highest at pH 7 (95%). Our results are consistent with those reported in Saleh [16] at pH 7, the Shell's seeds of *Ziziphus spina christi* adsorbed 91.1% of malachite green dye.

Influence of the temperature on MG adsorption

The temperature is considered an important factor and can be attributed to the efficiency of adsorption and removal of the MG. The effect of temperature on dye discoloration was evaluated preparing a mixture of MG with raw benonite, nano-bentonite and MgO-impregnated clay at different temperatures in the 25–70 °C range while keeping the adsorbent dosage (0.7 g), the pH (7), the contact time (60 min), and agitation speed (200 rpm) constant. As can be evinced from Fig. 7, evidence indicates that the rate of adsorption of MG onto nano-bentonite increased as the temperature was raised from 25 to 35 °C; At 25 °C, the percentage removal of MG was 92.2%; at 35 °C, this parameter increased to 99.8%; and the percent MG removal did not display any significant change until the temperature reached 70 °C. This evidence indicates that the adsorption process was slightly endothermic. A similar trend was reported by Al-asheh and Banat [24] for the removal methylene blue by activated bentonite. In contrast, the percent removal of MG by MgO-impregnated clay increased when the temperature was raised from 25 to 70 °C. At 25 °C, the percentage removal of the dye was 88.3%, at 50 °C, this value increased to 98.1%. The adsorption process was exothermic, as shown in (Fig. 7). On the other hand, the percent removal of MG by raw bentonite increased when the temperature was raised from 25 to 50 °C. At 25 °C, the percentage removal of the dye was 35.3%, while at 45 °C, this value increased to 70.7%. Indeed, the increase in percentage removal is observed, because the kinetic energy of the molecules increases as the temperature increases, and the accelerated molecules disperse faster in the adsorbent [55]. In addition, the increased temperature will cause the internal structure of the adsorbent to swell, allowing large dyes to penetrate the adsorbent [56]. This finding was consistent with the data reported by Saleh [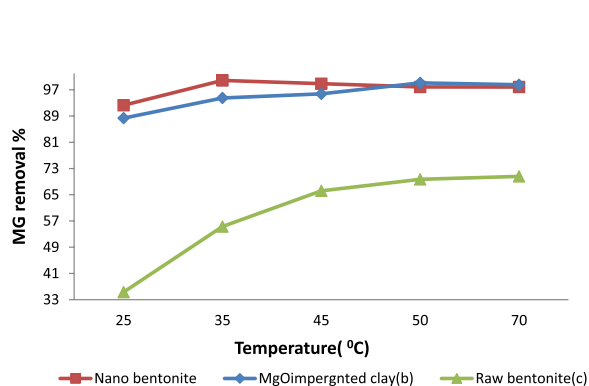16], who found that the value for MG removal with activated carbon prepared from shells seeds increased up to 95% as a result of the temperature being raised to 50 °C. Fabryanty [37], stated that the crystal violet dye removal with bentonite–alginate composite increased up to 98.2% as a result of the temperature being raised to 60 °C. Chauhdary et al. [57] reported the adsorption of directviolet-51, on pure bentonite and bentonite clay nanocomposites prepared using potassium ferricyanide for which the maximum removal efficiency were found to be 96.6% and 80% at 50^0C, respectively.

Influence of contact time on MG adsorption

Assessing the effect of the contact time is important, because the results of such an investigation provide basic information on how quickly the adsorption process reaches equilibrium. The effect that changing the contact time in the 10–60 min range had on the adsorption capacity was studied, while other parameters were kept constant (adsorbent dosage, 0.7 g, pH 7, initial MG concentration, 50 mg/L, agitation speed, 200 rpm and temperature, 35 °C). Based on the results reported in Fig. 8, rapid dye adsorption was observed in the initial phase of the experiment; subsequently, dye adsorption gradually slowed down, as the equilibrium condition was approached after about 60 min. In the case of nano-bentonite, at the 10 min, the percentage removal of MG was 90.9%, and the value for this parameter gradually increased to 95.3% at the 20 min and to 98.2% at the 60 min. In the case of the MgO-impregnated clay, the MG percentage removal was 89.8% at the 10 min; it increased sharply to 95.9% at the 30 min, and to 98.2% at the 60 min. In contrast, in the case of raw bentonite, at the 10 min, the percentage removal of MG was 44.2%, and the value for this parameter gradually increased to 70.06% at the 60 min. In fact, the maximum removal efficiency achieved by nano-bentonite was 98.8%, whereas that achieved by MgO-impregnated clay was 98.2%. The

Fig. 7 Effect of temperature on MG dye removal by **a** nano-bentonite, **b** MgO impregnated clay and **c** raw bentonite
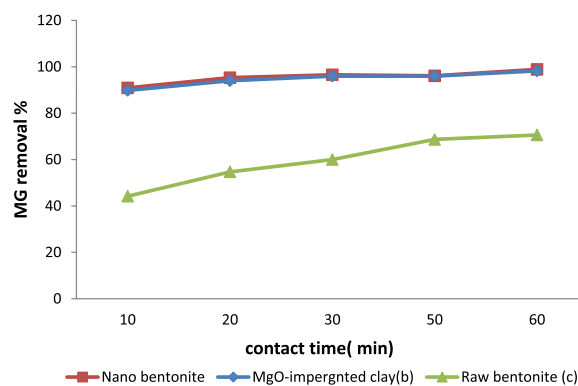

Fig. 8 Effect of contact time on MG dye removal by **a** nano-bentonite, **b** MgO impregnated clay and **c** raw bentonite

time required to reach equilibrium in the adsorption of MG on nano-bentonite and on MgO-impregnated clay was found to be 30 min. The described trend could be rationalized by envisioning a situation, whereby MG molecules proceeded to occupy a large number of initially vacant active sites on the surfaces of the adsorbents, resulting in a high initial adsorption rate; as the contact time increased; however, the MG adsorption rate decreased as the number of vacant sites decreased and the repulsive forces between the dye molecules adsorbed on the biomass increased, and the large phase led to a significant decrease in absorption capacity, so that the dye molecules slowly diffused into the interior of the adsorbents [58]. The results of the present study are consistent with those reported by Tarekegn and Balakrishnan [3] on the effects of contact time on the adsorption of methylene blue dyes on nano-zero-valent iron, nano-clay, and iron-impregnated nano-clay [58]. Present study is consistent with previous literature [3] who, reported that the effects of contact time on the adsorption of malachite green dye on the titanium coated graphite with CNT-ABS adsorbents achieved removal efficiency at 35%, (20 min) and it increased to 97.3% at 60 min.

Influence of the initial MG concentration on dye adsorption
The effect of the initial concentration of MG on its adsorption on nano-bentonite, raw bentonite and MgO-impregnated clay was investigated by making the said concentration vary in the 50–250 mg/L, range, while the other parameters were kept constant (contact time, 60 min; pH 7; initial concentration, 50 mg/L; agitation speed, 200 rpm and temperature, 35 °C). The dye removal efficiency of the adsorbents declined as the initial concentration of MG increased. Notably, the dye adsorption activity of MgO-impregnated clay was less influenced by changes in the initial concentration of the adsorbate than nano-bentonite. The MG removal efficiency of

MgO-impregnated clay declined from 96.7% to 89.7% and raw bentonite declined from 70.06% to 55.3% as the initial MG concentration increased from 50 to 250 mg/L (see Fig. 9). While nano-bentonite achieved a maximum MG removal efficiency of 98.6% at an initial concentration of MG of 50 mg/L, this parameter's value was reduced to 91.5% when the initial concentration of MG increased to 250 mg/L. This trend can probably be explained considering that the lower the initial concentration of MG, the larger the proportion of initially vacant (available) active sites on the surface of the adsorbent. Fairly similar observations were reported by Jinendra et al. [54] and Puchongkawarin et al. [1]. Our results were in agreement with the previous study by Tarekegn and Balakrishnan [3], which found that the iron impregnated clay's ability to remove MB dye from 98.86% to 76.80% at doses of 20–80 mg/L, respectively.

Influence of adsorbent dosage on MG adsorption
The dosages of nano-bentonite, MgO-impregnated clay and raw bentonite were another crucial factor influencing dye adsorption activity. The dosages of nano-bentonite and MgO-impregnated clay and raw bentonite were made to have the following values: 0.1, 0.2, 0.5, 0.7, 1 and 1.2 g; in the experiments conducted, the initial MG concentration (50 mg/L), temperature (35 °C), agitation speed (200 r/min), and pH (7) were kept constant. As can be evinced from in Fig. 10, the dosages of nano-bentonite, MgO-impregnated clay and raw bentonite that afforded the maximum rate of MG removal were 1.0, 0.7 and 1.2 g, respectively. The maximum MG removal efficiency achieved by nano-bentonite was 98.6% and that achieved by MgO-impregnated clay was 97.4%. The MG adsorption rate of MgO-impregnated clay increased sharply from 48.1% measured at a 0.05 g dosage of MgO-impregnated clay to 97.8% at a 0.7 g dosage of the said
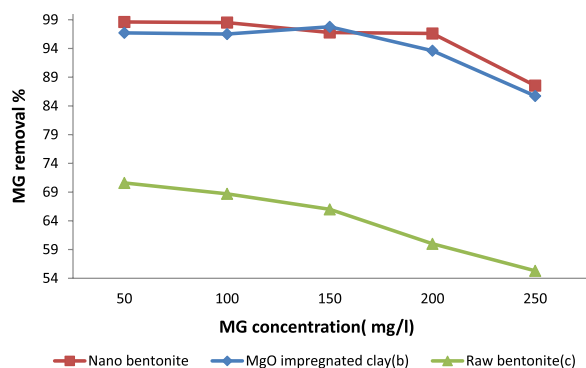

Fig. 9 Effect of initial MG dye concentration on MG dye removal by **a** nano-bentonite, **b** MgO impregnated clay and **c** raw bentonite
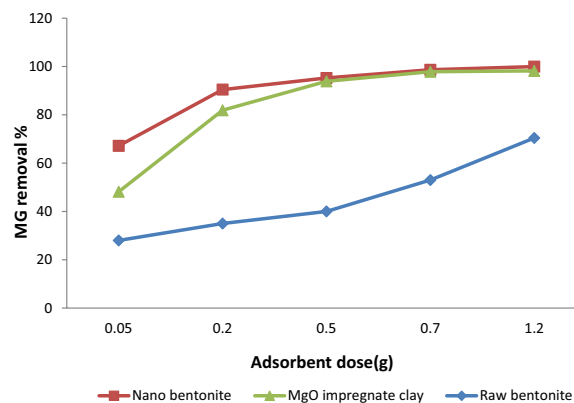

Fig. 10 Effect of adsorbent dose on MG dye removal by **a** nano-bentonite, **b** MgO impregnated clay and **c** raw bentonite

adsorbent. The adsorption efficiency of MgO-impregnated clay then increased gradually to 98.1% at a 1.0 g dosage. By contrast, nano-bentonite exhibited a higher adsorption rate than MgO-impregnated clay at a 0.05 g dosage (67.1%) and a more gradual increase in adsorption efficiency as its dosage increased to 0.7 g (adsorption rate: 99.8%). The MG removal efficiency remained constant as the adsorbent dosage was made to increase further to 1.0 g (Fig. 10). On the other hand, the adsorption efficiency of raw bentonite increased gradually from 28.1% to 70.4% at 0.05–1.2 g dosage, respectively. The results of these experiments were consistent with those reported by Mortazavi et al. [59], which indicated that the initial concentration of MG was inversely proportional to the efficiency of MG adsorption on silver nanoparticles coated on activated carbon. Akpomie and Conradie [7, 8], who found that the adsorption of malachite green increased from 52.6 to 100%, as the Prosopis cineraria dose was increased from 0.2 to 1.0 g/100 mL at equilibrium time.

Optimization of adsorption by Box–Behnken design

To optimize the adsorption process, a Box–Behnken design with four factors (initial concentration of dye, temperature, adsorbent dose, and pH) was chosen. The higher and lower levels of the variables are listed in Table 2, while the experimental and predicted values of the percentage decolorization of MG in the presence of nano-bentonite and MgO-impregnated clay are listed in Table 3. The second-order response surface polynomial function [Eqs. (11) and (12)] can be used to predict the dye's optimum operating circumstances:

$$
\begin{aligned}
Y(\text{nano - bentonite}) =\ & 97.3092 + 2.839 * A + -0.72275 * B \\
& + 0.0690833 * C + -0.0521667 * D \\
& + 0.69575 * AB + -0.67425 * AC \\
& + 0.321 * AD + -1.136 * BC \\
& + 0.8515 * BD + -0.4435 * CD \\
& + -2.37618 * A^2 + -0.276058 * B^2 \\
& + -0.215808 * C^2 + 0.0813167 * D^2
\end{aligned}
$$

$$(11)$$

Table 2 Experimental range and levels of input process variables assessed

Variables	Code	Levels		
		−1	0	1
pH	A	5	7	9
Dye concentration (mg/L)	B	5	50	100
Temperature (°C)	C	30	35	40
Dosage (g/L)	D	2.0	4.0	6.0

$$
\begin{aligned}
Y(\text{MgO - impregnatedclay}) \\
=\ & 97.4599 + 1.08619 * A \\
& + -0.952475 * B + -0.0289832 * C \\
& + -0.830585 * D + 0.964158 * AB \\
& + -1.15204 * AC + -1.9757 * AD \\
& + 1.0302 * BC + 0.528359 * BD \\
& + -0.482124 * CD + -3.78607 * A^2 \\
& + -0.135132 * B^2 + -0.163015 * C^2 \\
& + 0.188028 * D^2
\end{aligned}
$$

$$(12)$$

The assessment of variance (ANOVA) for MG elimination efficiency in the cases of nano-bentonite and MgO-impregnated clay was applied to validate the model, as given in Table 4(a, b). The correlation between the variables and the responses was determined using the quadratic model and second-order polynomial analysis. The Model *F*-values of MG removal percentage achieved by nano-bentonite and MgO-impregnated clay were recorded as 71.81and 36.85, respectively, which were favorable. The model *p*-values of both models for MG removal were acceptable. Model terms are considered significant when the *p*-value is less than 0.0500. In this case, A, B, D, AB, AC, AD, BC, and A^2 are significant model terms for MgO-impregnated clay. When the value was higher than 0.1, model terms were not considered significant. On the other hand, the model *F*-value of nano-bentonite was 71.81, indicating that the model was favorable. In this case, A, B, AB, AC, AD, BC, BD, CD, and A^2 were satisfied model terms. The lack of fit *F*-value of nano-bentonite and MgO-impregnated clay were 2.62 and 0.29, respectively, implies the lack of fit is not significant relative to the pure error. There was a 22.64% and 94.48% chance for nano-bentonite and MgO-impregnated clay, respectively that a lack of fit *F*-value this large could be due to noise. A non-significant lack of fit indicated that the quadratic model was fit for the present study. The second-order polynomial equation was developed based on these findings to indicate a relationship between MG elimination percentage and a number of different variables. Only 0.2% and 0.9% of the total variation could not be explained by the model, according to the regression equation derived after the ANOVA, which indicated that the correlation coefficient (R^2) values for the MG dye removal by nano-bentonite and MgO-impregnated clay were 0.986 and 0.973, respectively. A high R^2 value (close to 1) indicates that the calculated and observed findings within the experimental range are in good agreement with each other, and it also demonstrates that an acceptable and reasonable agreement with adjusted R^2. The predicted R^2 values for nano-bentonite and MgO-impregnated clay were 0.929 and 0.91,

Table 3 Experimental design and results of the Box–Behnken design for the decolourization of MG by nano-bentonite and MgO impregnated clay

Run	pH	Concentration	Temperature	Dosage	Nano-bentonite	MgO impregnated clay
1	0	0	0	0	97.13	90.08
2	−1	0	0	−1	92.429	91.41
3	0	0	0	0	97.212	93.71
4	0	0	0	0	97.114	96.6
5	0	1	0	1	97.212	97.32
6	1	0	0	1	98.409	97.2
7	0	−1	0	1	96.51	98.95
8	0	1	1	0	96.118	97.18
9	−1	0	1	0	92.401	93.05
10	0	1	0	−1	96.016	96.41
11	1	0	0	−1	97.392	93.89
12	0	0	1	−1	98.05	97.91
13	0	−1	0	−1	98.72	97.01
14	0	0	−1	−1	96.413	97.85
15	0	0	−1	1	97.119	98.85
16	−1	1	0	0	90.015	97.012
17	0	−1	1	0	98.812	94.91
18	1	0	1	0	96.47	95.81
19	0	−1	−1	0	96.312	94.81
20	−1	0	0	1	90.062	97.51
21	−1	−1	0	0	92.32	94.15
22	1	−1	0	0	97.84	96.05
23	1	0	−1	0	98.382	95.029
24	0	0	0	0	97.3	92.0
25	−1	0	−1	0	89.616	96.94
26	0	1	−1	0	97.162	92.04
27	0	0	0	0	97.8	98.51
28	0	0	1	1	96.982	99.77
29	1	1	0	0	97.318	90.08

respectively, which are reasonably consistent with the adjusted R^2 values: 0.952 and 0.947, respectively. These results demonstrated the effectiveness of the established model and the accuracy and minimal inaccuracy of the independent variable values. Adequate precision is used to determine of the signal to the noise ratio. A ratio larger than 4 is desirable. The values for this ratio were 29.5 and 22.842 for nano-bentonite and MgO-impregnated clay, respectively, indicating the reliability of the experimental data. The repeatability of the model is measured using a parameter called coefficient of variation (CV%), which is the ratio of the standard error of the estimate and the mean value of the observed response (expressed as a percentage). Typically, a model is regarded as replicable if its CV% value is less than 10% [60]. According to the data listed in Table 4(a, b), the CV% values of nano-bentonite and MgO-impregnated clay are relatively small, 0.4 and

0.5%, respectively, which indicated that the deviations between experimental and predicted values were low. The plots between experimental (actual) and predicted values of MG removal by RSM model are reported in Fig. 11a, b. Based on this figure, the average differences between the predicted and experimental values can be evinced to be less than 0.1, which indicates that most of the regression model provided an explanation for the data variation.

Interpretation of variable interaction on MG removal

Three-dimensional surface plots and contour plots were generated to investigate the interaction between MG removal efficiency and two parameters at a time, while the other variables were held at constant values. The data reported in Figs. 12a, b and 13a, b demonstrate unequivocally that, as the temperature increased, so did decolorization percentage along with increasing

Table 4 Analysis of variance (ANOVA), results for decolourization of MG by (a) nano-bentonite, (b) MgO impregnated clay

Source	Sum of squares	df	Mean square	F-value	p-value	
(a)						
Model	154.80	14	11.06	71.82	< 0.0001	Significant
A-pH	96.72	1	96.72	628.26	< 0.0001	
B-Concentration	6.27	1	6.27	40.72	< 0.0001	
C-Temperature	0.0573	1	0.0573	0.3720	0.5517	
D-Dose	0.0327	1	0.0327	0.2121	0.6522	
AB	1.94	1	1.94	12.58	0.0032	
AC	1.82	1	1.82	11.81	0.0040	
AD	0.4122	1	0.4122	2.68	0.1241	
BC	5.16	1	5.16	33.53	< 0.0001	
BD	2.90	1	2.90	18.84	0.0007	
CD	0.7868	1	0.7868	5.11	0.0402	
A^2	36.62	1	36.62	237.90	< 0.0001	
B^2	0.4943	1	0.4943	3.21	0.0948	
C^2	0.3021	1	0.3021	1.96	0.1830	
D^2	0.0429	1	0.0429	0.2786	0.6059	
Residual	2.16	14	0.1539			
Lack of fit	1.83	10	0.1831	2.26	0.2246	Not significant
Pure error	0.3243	4	0.0811			
Cor total	156.96	28				
SD	0.3924					
Mean	96.16					
CV %	0.4080					
R^2	0.9863					
Adjusted R^2	0.9725					
Predicted R^2	0.9296					
Adeq precision	29.5754					
(b)						
Model	164.92	14	11.78	36.85	< 0.0001	Significant
A-A	14.16	1	14.16	44.29	< 0.0001	
B-B	10.89	1	10.89	34.06	< 0.0001	
C–C	0.0101	1	0.0101	0.0315	0.8616	
D-D	8.28	1	8.28	25.90	0.0002	
AB	3.72	1	3.72	11.63	0.0042	
AC	5.31	1	5.31	16.61	0.0011	
AD	15.61	1	15.61	48.84	< 0.0001	
BC	4.25	1	4.25	13.28	0.0027	
BD	1.12	1	1.12	3.49	0.0827	
CD	0.9298	1	0.9298	2.91	0.1102	
A^2	92.98	1	92.98	290.86	< 0.0001	
B^2	0.1184	1	0.1184	0.3705	0.5525	
C^2	0.1724	1	0.1724	0.5392	0.4749	
D^2	0.2293	1	0.2293	0.7174	0.4112	
Residual	4.48	14	0.3197			
Lack of fit	1.91	10	0.1914	0.2988	0.9448	Not significant
Pure error	2.56	4	0.6404			
Cor total	169.40	28				
SD	0.5654					
Mean	95.85					

Table 4 (continued)

Source	Sum of squares	df	Mean square	F-value	p-value
CV %	0.5899				
R^2	0.9736				
Adjusted R^2	0.9472				
Predicted R^2	0.9113				
Adeq precision	22.8424				

pH. The maximum removal of MG dye decolorization from 25 to 35 °C, for nano-bentonite and 25–50 °C for MgO-impregnated clay, with increasing pH 7.0 and pH 9.0, there was a rise in the percentage of decolorization, respectively. The elliptical shape of the curve is indicative of a high degree of interaction between the three variables. When the interaction of the MG removal efficiency with the adsorbent dosage and the adsorption temperature was examined, it was discovered that this analysis's affecting factor was temperature, as can be evinced from Figs. 12c, d and 13c, d. As the adsorbents' dosage increased, so did the rate of MG decolorization. The temperature was found to be most influential at an nano-bentonite dosage of 0.2 g/L, in which casea 79% decolorization could be observed at 25 °C and 98% decolorization could be observed at 35 °C. Maximum decolorization could be observed at a temperature of 35 °C and adsorbent dosage of 1.0 g/L. On the other hand, maximum decolorization of MG afforded by MgO-impregnated clay could be observed (97%) at a temperature of 50 °C. The data reported in Figs. 12e, f and 13e, f reflect the effect that the pH and the initial MG concentration had on the percentage of MG removed, in conditions, whereby the temperature was kept constant. Above a specific initial MG concentration (above 300 mg/L), the adsorption capacity declines as the initial MG concentration increases, but there was a net positive interaction effect, suggesting that the adsorption capacity increases as the initial MG concentration and initial pH increase. The maximum capacities for MG adsorption by nano-bentonite and MgO-impregnated clay were observed at pH values in the 7.0–9.0 range. Thus, evidence indicates that the percentage of noxious dye elimination afforded by nano-bentonite and MgO-impregnated clay was very low at acidic pH 5.0. Referring back to Figs. 12 and 13, the combined effect on MG removal efficiency of changing the adsorbent dosage and the initial MG concentration were investigated, in conditions, whereby the temperature and pH were fixed at zero level. As can be evinced from Fig. 12, more than 98% and 90% of the MG dye was removed in the presence of nano-bentonite and MgO-impregnated clay

under the mentioned conditions, respectively. Notably, the maximum MG removal percentage was obtained at high adsorbent dosage (0.7 g/L for nano-bentonite) and (1.0 g/L for MgO-impregnated clay), and minimum dye concentration (100 mg/L). As can be evinced from Figs. 12 and 13, dye adsorption decreased as the initial MG concentration increased. This trend may be due to the fixed number of active sites on the adsorbent vis-à-vis an increasing number of dye molecules. [61] reported that the efficiency of dye adsorption on the adsorbents dropped significantly as the initial adsorbate concentration increased.

Kinetic adsorption for MG removal

Kinetic studies on the adsorption of MG onto raw bentonite, nano-bentonite and MgO-impregnated clay were conducted by fitting the experimental data with pseudo-1st-order and pseudo-2nd-order reaction rate equations.

Pseudo-first-order kinetics fitting of MG adsorption data

The experimental kinetic data were fitted with the Lagergren pseudo-first-order rate equation (Eq. 13) [62, 63]:

$$\log (q_e - q_t) = \log q_e - \left(\frac{k_1}{2.303} \right) t \tag{13}$$

where k_1 is the pseudo-primary order rate constant (min^{-1}), q_e represents the amount of MG removed at time-point t (min) of adsorbent (mg/g), and q_t represents the MG adsorption capacity at equilibrium (mg/g). In Fig. 14a–c is reported the plot of $\log (q_e - q_t)$ versus time, whereas the relevant R^2 values and constant quantity for such various adsorption kinetic designs are listed in Table 5. Given the discrepancy between the calculated (q_e, cal) and experimentally determined (Exp q_e) adsorption capacities, which can be evinced from Table 5, a pseudo-first-order kinetics model was unable to explain the adsorption of MG onto nano-bentonite, raw bentonite and MgO-impregnated clay. In addition, when compared to the pseudo-second-order value, the values of the coefficient of determination (R^2) were relatively small at 0.975, 0.916, and 0.86 for the nano-bentonite, MgO-impregnated clay and raw bentonite cases, respectively.
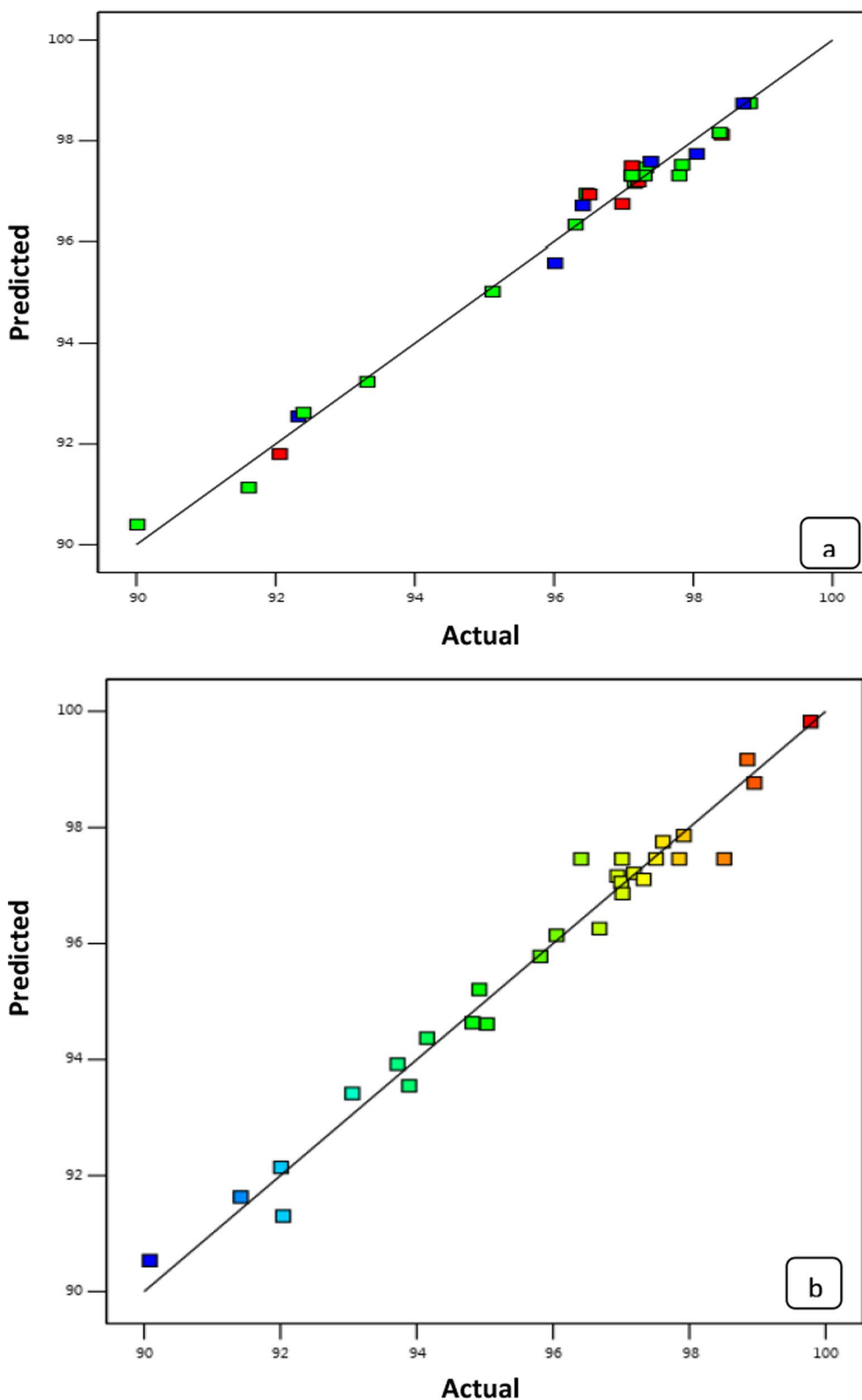
Fig. 11 Linear correlation between experimental and predicted removal efficiency % MG by **a** nano-bentonite and **b** MgO impregnated clay
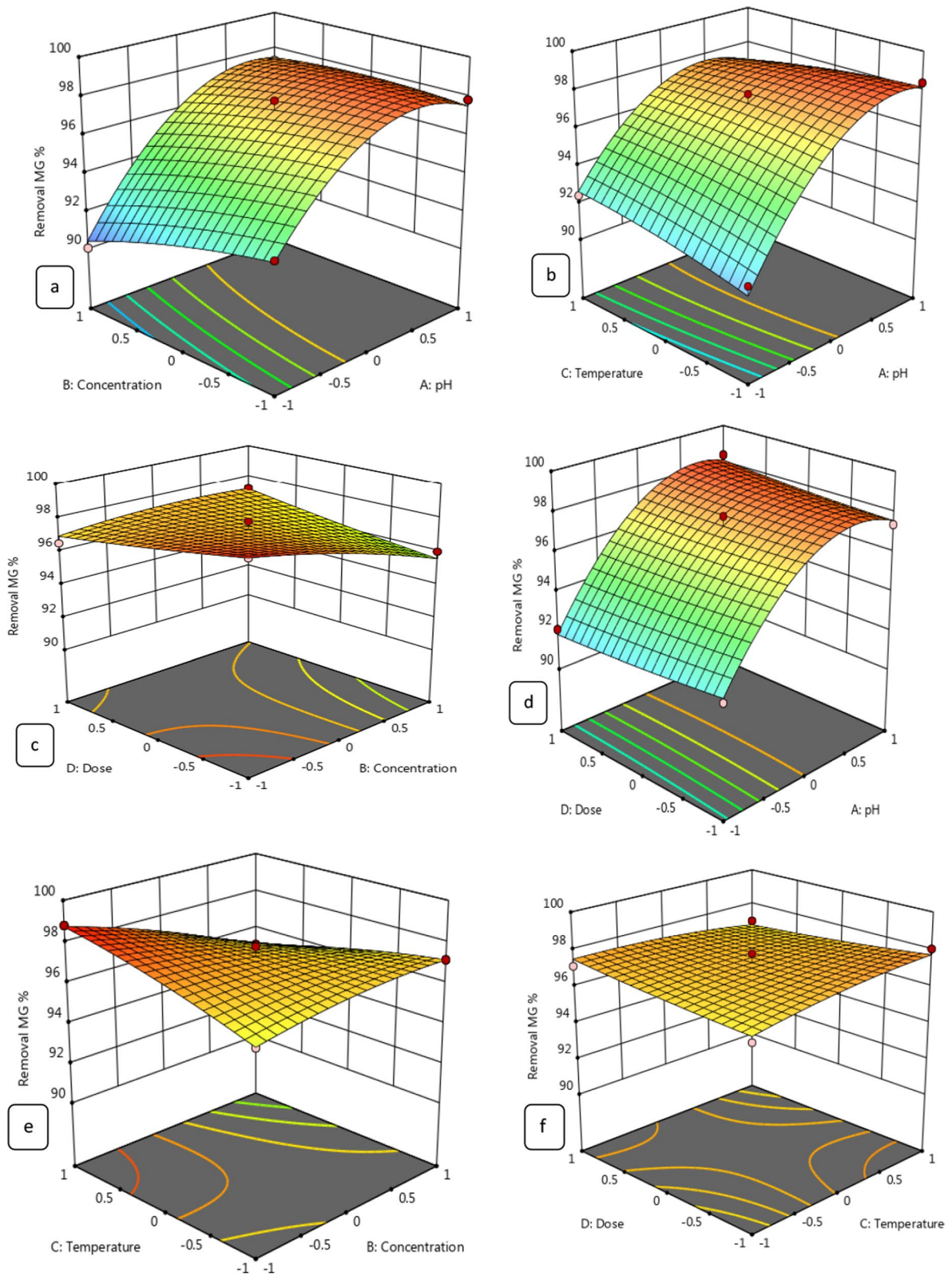
Fig. 12. 3D response surface plot of MG removal % through nano-bentonite as a function of pH, temperature and adsorbent dosage
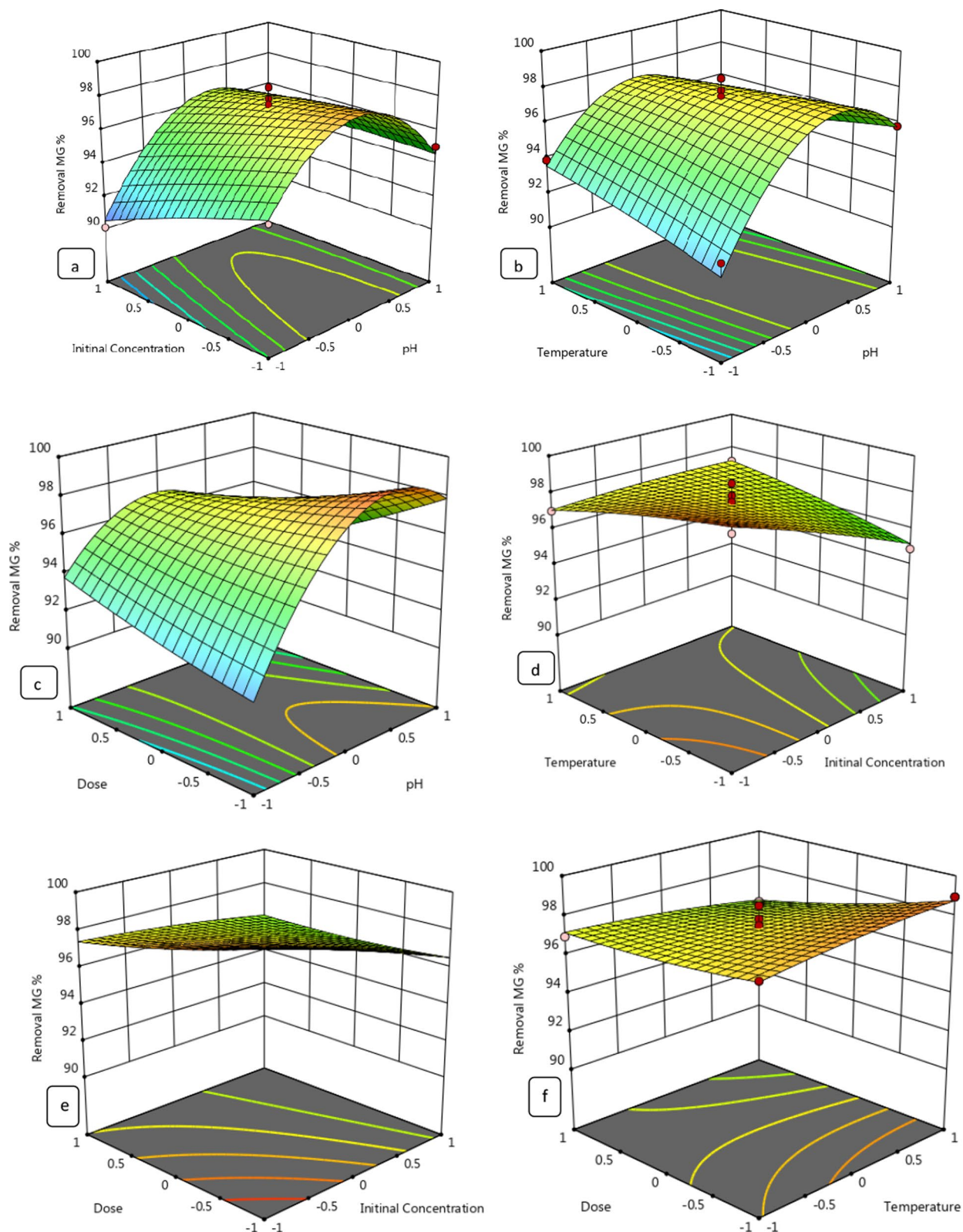
Fig. 13. 3D response surface plot of MG removal % through MgO impregnated clay as a function of pH, temperature and adsorbent dosage
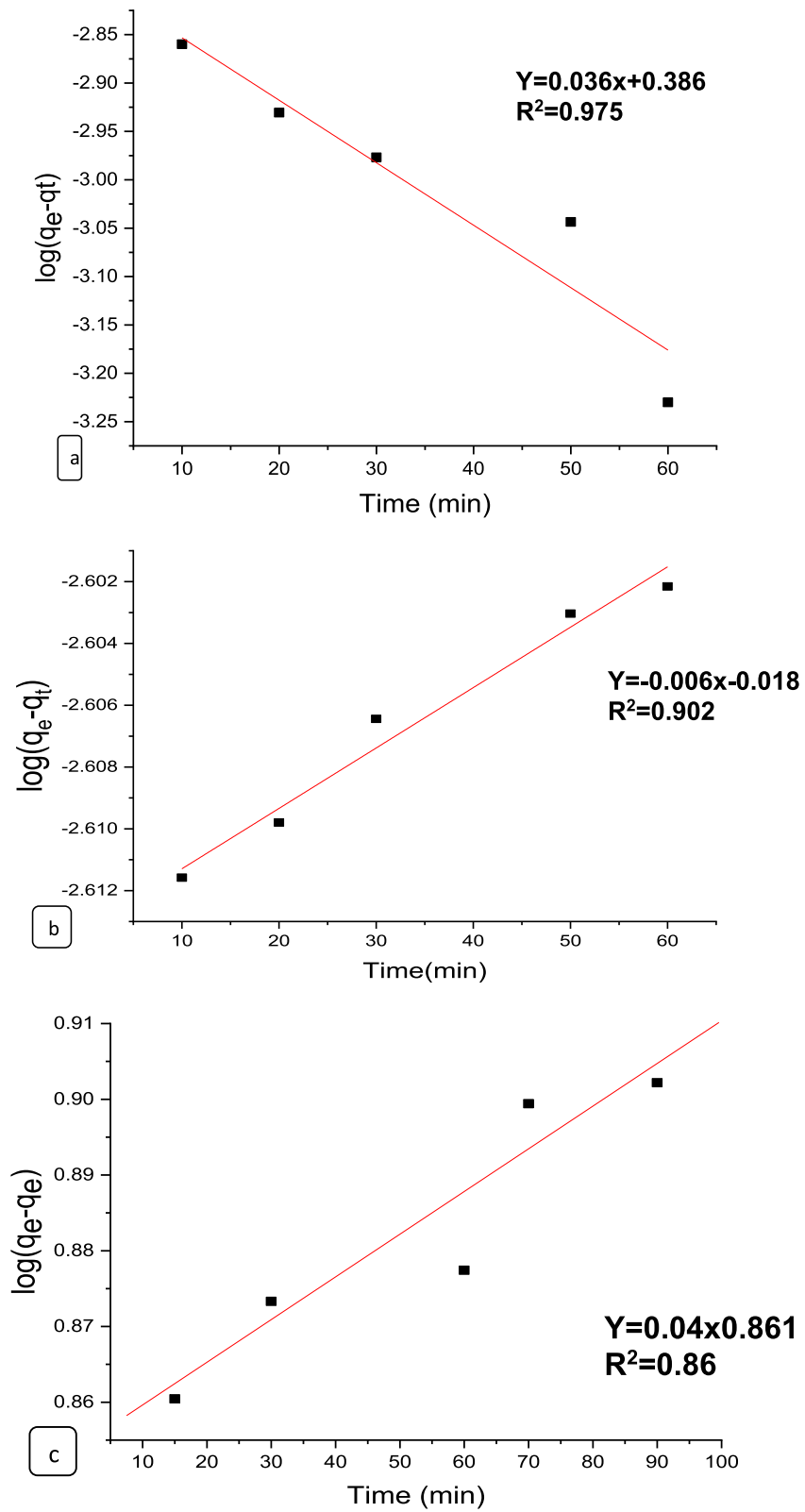
Fig. 14 Pseudo-first order for the adsorption of MG onto **a** nano-bentonite, **b** MgO impregnated clay and **c** raw bentonite

Table 5 Kinetic parameters for the adsorption MG onto nano-bentonite, MgO impregnated clay and raw bentonite

Model	Kinetic parameter	Nano-benonite	MgO-clay	Raw benonite
Pseudo first-order	qe1 cal. (mg/g)	2.4	1.01	7.1
	K1 (min^{-1})	0.08	6.5	0.09
	R^2	0.975	0.91	0.86
	qe2 exp. (mg/g)	0.21	0.0035	49
Pseudo second-order	qe2 cal. (mg/g)	0.398	0.00001	50
	$K2$ (min^{-1})	0.016	0.0036	0.01
	R^2	0.996	0.999	0.98

Pseudo-second-order kinetics fitting of MG adsorption data

The equation for the Lagergren pseudo-second-order kinetics (Eq. 14) is stated linearly as shown below [1, 63]:

$$\frac{t}{q_t} = \frac{1}{k_2 q_e^2} + \frac{1}{q_e} t \tag{14}$$

where k_2 is the pseudo-second-order rate constant of MG adsorption (gmg^{-1} min^{-1}), and t is the contact time (min). The fitness of the straight line (R^2) and the consistency between the experimental and calculated values of q_e serve as indicators of each model's validity.

The plot of t/q_t versus the contact time is reported in Fig. 15a–c, and the values for the relevant parameters (R^2, slope, intercept, pseudo-first order rate constant) "$K1$", and the experimental and calculated dye uptake levels) are listed in Table 5. As can be evinced from this table, the R^2 values for raw bentonite (0.988), nano-bentonite (0.996), and MgO-impregnated clay (0.999) were quite close to 1. The computed q_e values for both nanomaterials were in excellent agreement with the actual data, when the pseudo-second-order reaction rate equation was utilized for the computation. This observation indicates that the adsorption of MG on nano-bentonite, raw bentonite and MgO-impregnated clay proceeds through a mechanism described by a second-order kinetics equation. According to a study conducted by Taher et al. [64], the adsorption of the Congored dye onto acid-activated bentonite exhibits pseudo-second-order kinetics.

Thermodynamic study

The thermodynamic adsorption qualities depend greatly on temperature. The effect of adsorption temperature on the MG adsorption of nano-bentonite, raw bentonite and MgO-impregnated clay was investigated at various temperatures (298, 303, 308, 323, and 343 K). During the study on the thermodynamics of dye adsorption, 50 mg/L of dye and 1 g/L of two distinct adsorbents were used at temperatures of 25 °C, 30 °C, 35 °C, 50 °C, and 70 °C. The rate equation (15) and the van't Hoff equation can be used to calculate the thermodynamic parameters, such as changes

in the standard free energy (G), enthalpy (H), and entropy (S), related to the adsorption process (16). The rate equation is represented as follows [61, 65]:

$$\ln K_L = \frac{-\Delta H°}{RT} + \frac{\Delta S°}{R} \tag{15}$$

$$\Delta G° = \Delta H° - T \Delta S° \tag{16}$$

Here ΔG^0 is the free energy change of the sorption process (kJ/mol), and KC is the ratio of the equilibrium concentration of the MG ions on the adsorbent to the equilibrium concentration of the MG dye ions in the solution. R is the ideal gas constant (8.314 J/(mol K)), and T is the adsorption temperature in K. After plotting $\Delta G°$ against temperature, a linear relationship was achieved. The slope and intercept of the plot were used to compute the values of $\Delta S°$ and $\Delta H°$. The results showed that $\Delta G°$ calculated from 25 to 70 °C were all negative, indicating that the adsorption of MG solution onto nano-bentonite and MgO-impregnated clay was feasible and spontaneous. Furthermore, analyses of the change in enthalpy ($\Delta H°$) and entropy ($\Delta S°$) were performed using the linear relationship [Eq. (15)]. Figure 16a–c shows the thermodynamic plot of $\Delta G°$ versus T to calculate $\Delta H°$ and $\Delta S°$. Table 6 shows that the corresponding $\Delta H°$ and $\Delta S°$ values for malachite green adsorption onto nano-bentonite obtained from the intercept and slope of the plot were equal to -52.68 kJ/mol and -0.2089 kJ/mol·K, respectively. The negative value of ΔH^0 in nano-bentonite showed that the adsorption was exothermic and indicated the possibility of chemisorption. These results are consistent with previous reports on the adsorption of MG on AC of rubber seeds, where MG adsorption was a chemisorption process [53]. The $\Delta H°$ and $\Delta S°$ values for malachite green adsorption onto MgO-impregnated clay were 54.6 kJ/mol and 0.19 kJ/mol·K. On the other hand, the $\Delta H°$ and $\Delta S°$ values for malachite green adsorption onto raw bentonite were 25.88 kJ/mol and 15.26 kJ/mol K, respectively. Furthermore, a positive $\Delta H°$ value in MgO-impregnated clay and raw bentonite adsorbents
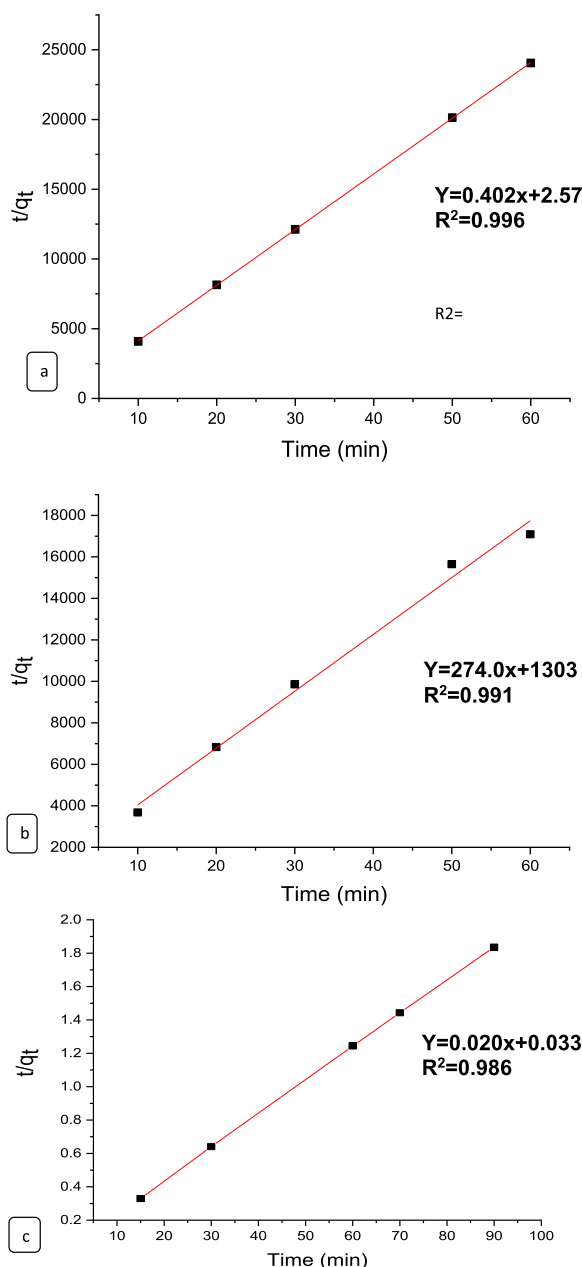
Fig. 15 Pseudo-second order for the adsorption of MG onto **a** nano-bentonite, **b** MgO impregnated clay and **c** raw bentonite
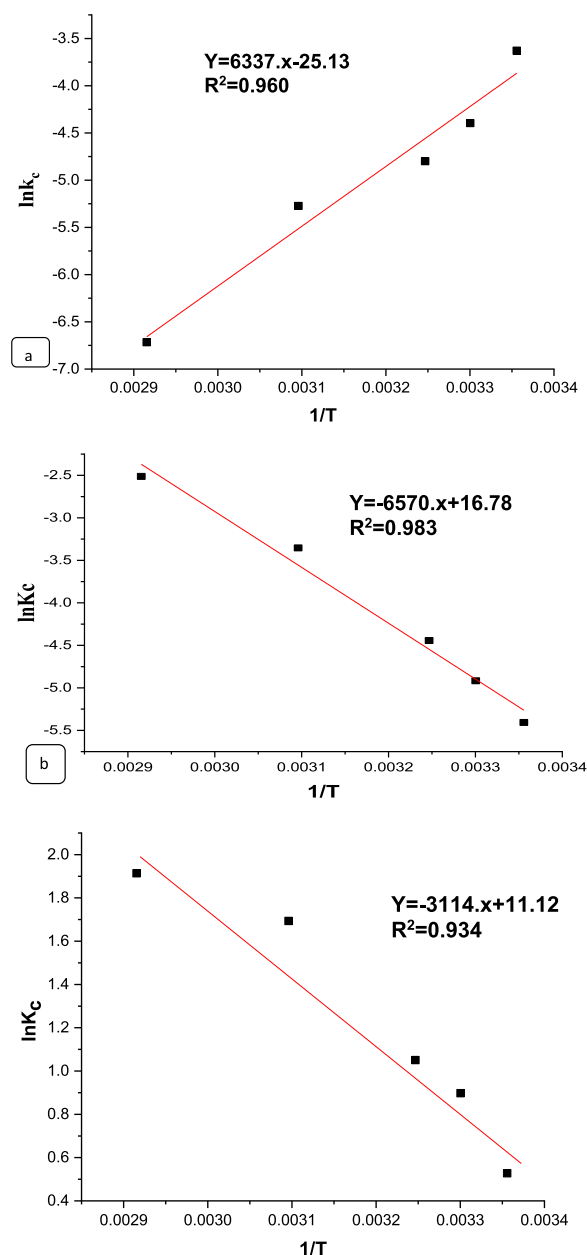

Fig. 16 Thermodynamic for the adsorption of MG onto **a** nano-bentonite, **b** MgO impregnated clay and **c** raw bentonite

activity showed that adsorption was endothermic and suggested the possibility of physisorption. The positive value of $\Delta S°$ indicates raise in randomness of solid–liquid interface during MG adsorption on MgO impregnated clay and raw bentonite [66]. This result is consistent with the findings in the section on the impact of temperature, which showed that adsorption capacity rises as temperature rises. In relation to $\Delta S°$, the positive value shows that modified-bentonite is a good MB solution adsorbent and that the solid-solution interface has increased unpredictability [67].

Adsorption isotherm

Studies on the adsorption isotherms, such as the Freundlich, Langmuir, and Temkin isotherms, can be used to examine the effectiveness of the adsorbent material used for adsorption. Moreover, they can be used to determine the nature of the interaction between the adsorbed matter and the adsorbent [68].

Table 6 Thermodynamic parameters of MG adsorption activity of nano-bentonite, MgO impregnated clay and raw bentonite

Adsorbent	Temperature (K)	DG (kJ mol^{-1})	DH (kJ mol^{-1})	DS (kJ mol^{-1})	R^2
Nano-bentonite	298	0.00957557	− 52.6858	− 0.20893	0.96
	303	0.01062022			
	308	0.01166487			
	323	0.01479884			
	343	0.01897745			
MgO impregnated clay	298	0.01304932	54.62298	0.13959	0.98
	303	0.01235178			
	308	0.01165423			
	323	0.0095616			
	343	0.00677142			
Raw bentonite	298	− 4.5229324	25.88	15.26	0.93
	303	− 4.5992549			
	308	− 4.6755774			
	323	− 4.904545			
	343	− 5.2098351			

Langmuir adsorption isotherm

According to Roy et al. [14], the Langmuir isotherm model was used to compute the maximal adsorption capacity resulting from complete monolayer coverage on the adsorbent surface and is shown as follows:

$$\frac{C_e}{q_e} = \frac{C_e}{Q_{max}} + \frac{1}{Q_{max}K_L} \tag{17}$$

Here, q_m is the monolayer adsorption capacity (mg g^{-1}), q_e is the equilibrium adsorption amount of the adsorbate, and C_e (mg/L) is the equilibrium adsorbate concentration. Regarding the adsorption rate (L/mg), K_L is the Langmuir isotherm constant. By charting C_e/q_e versus C_e, the values of q_m and K_L at various amounts of nano-bentonite and MgO-impregnated clay can be determined in the range of 0.99 and 1.2 L/mg, Fig. 17a–c. A dimensionless constant called the separation factor RL may be used to express the essential properties of a Langmuir isotherm. Table 7 shows the findings of MG removal on nano-bentonite, taw bentonite and MgO-impregnated clay using the Langmuir model. The R^2 in Table 7 showed strong positive proof of the adsorption of MG ion adsorbents following the Langmuir isotherm. The suitability of the linear form of the Langmuir model to nano-bentonite was confirmed through the high correlation coefficients $R^2 > 0.992$. Conversely, the linear form of the Langmuir model to MgO-impregnated clay and raw bentonite was slightly fit with the regression coefficients (R^2) value (96.3%) and (0.952%), respectively. This shows that the Langmuir isotherm can provide a decent sorption model. Moreover, the adsorption capacities of the nano-bentonite and MgO-impregnated clays were 13.8 mg/g, 17.2 mg/g, 10.20 mg/g, respectively. This result corresponds with Vergis et al. [4], who discovered that the adsorption capacity of $CuFe_2O_4$ for MG was 22 mg/g.

Freundlich adsorption isotherm

According to the Freundlich isotherm model, adsorption occurs on a heterogeneous surface with a non-uniform heat distribution over the adsorbent surface. The linearized form of the Freundlich model is given as follows [69]:

$$\ln q_e = \ln K_F + \frac{1}{n} \ln C_e \tag{18}$$

Here q_e is the amount adsorbed per unit mass of the adsorbent, C_e is the equilibrium concentration, and $1/n$ and K_F are the Frendulich constants. The values of $1/n$ represent the nonlinearity of the relationship between adsorption and solution concentration. Adsorption is linear if n equals unity, chemical adsorption is implied if the value of n is below unity, and advantageous physical adsorption is implied if n is above unity. Figure 18a–c shows the plots of $\ln q_e$ versus $\ln C_e$ for the adsorption of MG dye on nano-bentonite, raw benonite and MgO-impregnated clay. The values of K_F (mg/g) and n are obtained from the intercept and slope, respectively. The values were (1.9 mg/g) and (2.3) for nano-bentonite, (3.6 mg/g) and (1.3) for MgO-impregnated clay, and (5.09 mg/g) and 1.36 for raw benonite. The R^2 values for nano-bentonite, MgO-impregnated clay and raw bentonite are approximately 0.973, 0.982, and 0.84, respectively. This indicates that both systems are favorable and that the MgO-impregnated clay has a higher adsorption
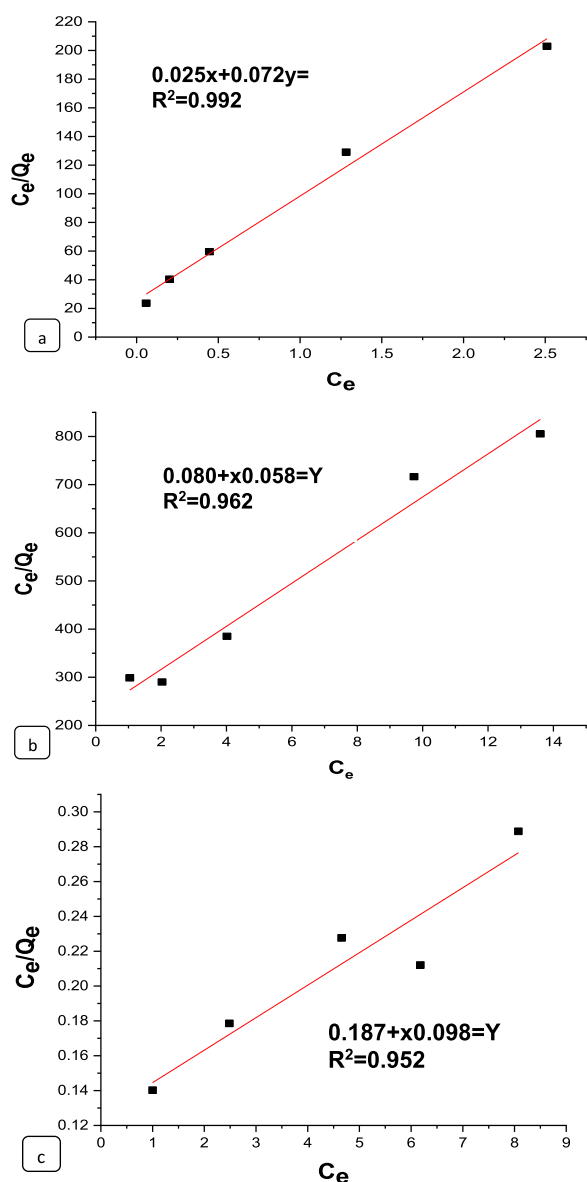
Fig. 17 Langmuir **a** nano-bentonite, **b** MgO impregnated clay and **c** raw bentonite plots for adsorption of MG

Table 7 Equilibrium isotherm modeling of MG adsorption onto adsorbents nano-bentonite, MgO impregnated clay and raw bentonite

Isotherm	Nano-bentonite	MgO-clay	Raw bentonite
Langmuir			
qe (mg/g)	13.8	17.2	10.27
R^2	0.992	0.962	0.952
Freundlich			
N	2.3	1.3	1.36
KF (L/mg)	109.5	3.6	5.09
R^2	0.973	0.982	0.84
Tempkin			
B (J/mol)	0.005	0.004	11.11
A_T (L/mg)	4.055	2.11	23.12
R^2	0.965	0.982	0.945

diverse mixes were assessed using the Tempkin adsorption isotherm. The R^2 value and decreased error analysis were effective and efficient criteria. The model has typically been used in the following format [Eq. (19)]:

$$q_e = \frac{RT}{b} \ln(K_T) + \frac{RT}{b} \ln(C_e) \qquad (19)$$

Here $\beta = (RT)/b$, T is the absolute temperature in Kelvin, and R is the universal gas constant [8.314 J (mol K)$^{-1}$]; the constant β correlates with the heat of adsorption [68]. As shown in Table 7 and Fig. 19a–c, applying the experimental equilibrium data to Eq. 19 demonstrated excellent and reasonable applicability of the model in explaining and interpreting MG adsorption on nano-bentonite, raw bentonite and MgO-impregnated clay. In the Temkin isotherm, positive AT values of 1.4 L/mg, 2.1 L/mg and 23.12 for nano-bentonite, MgO-impregnated clay and raw bentonite, respectively, showed that the process was endothermic. The Temkin model also showed a high R^2 value, indicating a chemisorption process rather than a physisorption one. The results obtained correspond with those reported by Gündüz [68]. Furthermore, the R^2 values realized using the Tempkin model were similar to those observed using the Langmuir and Freundlich equations.

Comparison of the adsorption capacities of nano-bentonite and MgO-impregnated clay with various adsorbents

In Table 8, the maximum adsorption capacities (q_{max}) of nano-bentonite and MgO-impregnated clay for MG adsorption are compared to the q_{max} of other adsorbents in the literature. The maximum adsorption capacities of MgO-impregnated clay and nano-bentonite for MG are shown to be greater than those of other adsorbent materials, which may be attributed to the strong adsorption
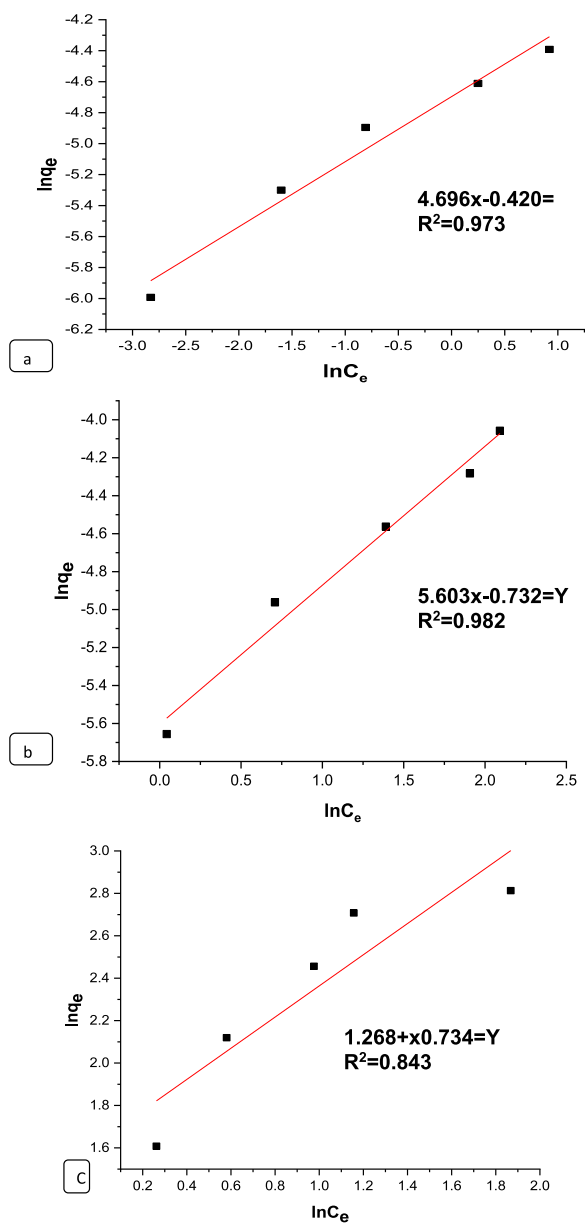
capacity. Therefore, the value of $1/n$ showed the applicability of the adsorbent used over the range of dye solution concentrations that significantly affect the Freundlich adsorption isotherm. The values of n for the MG dye adsorption on nano-bentonite, raw bentonite and MgO-impregnated clay were 2.3 g L^{-1}, 1.6 g L^{-1}, and 1.36 g L^{-1}, respectively, indicating that the adsorption occurred as a chemical process for $n > 1$.

Tempkin isotherm

The adsorption energy changes and the surface of the adsorbent toward the adsorption of different species in

Fig. 18 Freundlich **a** nano-bentonite, **b** MgO impregnated clay and **c** raw bentonite plots for adsorption of MG

Fig. 19 Temkin **a** nano-bentonite, **b** MgO impregnated clay and **c** raw bentonite plots for adsorption of MG

capacity of nano-bentonite. In addition, because the adsorbent surface was negatively charged during the experiment, the electrostatic attraction between positively charged adsorbate species and adsorbent particles grew, which caused additional MG to be adsorbed.

Parameters for the performance and optimization of MG adsorption

Analyzing the interaction between working factors using conventional methods is challenging. Consequently, predictions of operati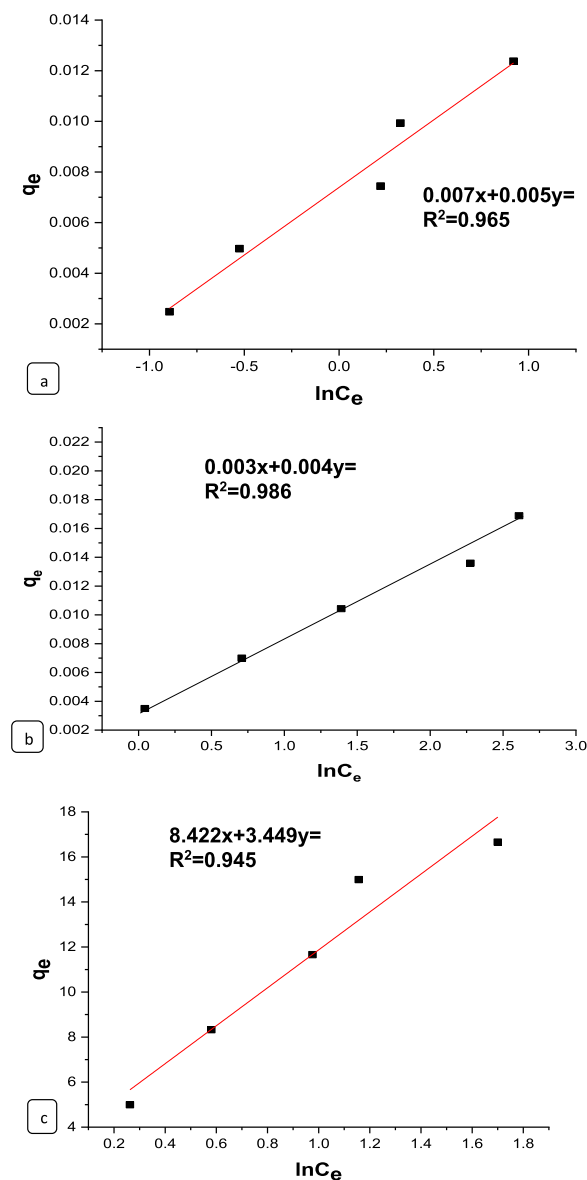onal factors and their synergistic impact are frequently based on assumptions. Operational factors can be simultaneously and efficiently analyzed, and the degree of interaction can be assessed using RSM. Due to the operational factor screening, the ideal conditions for MG adsorption were determined. The optimum condition of processing factors for MG adsorption was obtained at pH 9, with an initial concentration of 50 mg/L and a 4.0 g/L adsorbent dosage within 35 °C for nano-bentonite. Compared with MgO-impregnated clay, the optimum condition of processing factors was obtained at pH 9, with an initial concentration of 50 mg/L and 4.0 g/L adsorbent dosage within 40 °C. Under these

Table 8 Adsorption capacities of different adsorbents previously reported for the removal of MG compared with nano-bentonite and MgO impregnated clay

Adsorbents	Adsorption capacity (mg/g)	Removal percentage (%)	References
Shells seeds of Ziziphus spina christi	48.7	99.5	Bashanaini [16]
Nano-bentonite	13.8	98.6	Present study
MgO impregnated clay	17.2	97.04	Present study
Prosopis cineraria saw dust treated by Sulphuric acid	65.8	99.9	Garg et al. [81]
NaOH-modified breadnut peel	352.2	90	Chieng et al. [53]
Alg-Fe$_3$O$_4$ nanoparticles	47.8	99.9	Mohammadi [84]
coal-associated soil	89.9	96.7	Sundararaman et al. [85]
Sea shell powder	42.3	93.2	Chowdhury and Saha [82]
Organically modified hydroxyapatite	188.5	98.3	El-Zahhar and Awwad [86]
Calcium alginate nanoparticles	277.7	98.5	Geetha et al. [83]

Table 9 Experimental range and levels of input process variables assessed

Variables	Code	Levels		
		−1	0	1
Ph	A	5	7	9
Dye concentration (mg/L)	B	5	50	100
Temperature (°C)	C	30	35	40
Contact time (h)	D	24	48	72

circumstances, the high decolorization efficiency was 97.53% and 93.9% for nano-bentonite and MgO-impregnated clay, respectively.

Optimization of malachite green decolorization using statistical design

Table 9 shows that the Box–Behnken design with four variables (pH, initial concentration, contact time, and temperature) was used to improve the decolorization process. Table 10 shows the experimental and predicted values of the percentage decolorization. The second-order response surface polynomial function allowed the prediction of ideal dye operating conditions. Figure 20a, b shows that the experimental response values for MG decolorization correspond with the predicted response values, the normal probability, and the studentized residual plot.

$$Y = 87.98 + 2.09167 * A + -0.153333 * B$$
$$+ -0.0158333 * C + 1.53917 * D$$
$$+ -2.5 * AB + -7.25 * AC + 1.575 * AD$$
$$+ 4.61 * BC + -7.265 * BD + 0.0925 * CD$$
$$+ -18.4612 * A^2 + -9.34375 * B^2$$
$$+ -5.145 * C^2 + -4.3425 * D^2$$

$$(20)$$

According to Table 11, the ANOVA results for the quadratic regression model indicated that the model was significant. The superior *F* value (60.99) and reduced *P* values (< 0.0500) of malachite green show that the model terms were significant. The variables A, D, AB, AC, BD, BD, A2, B2, C2, and D2 were determined to be significant model terms for decolorization based on the *P* values. Furthermore, according to the results of the ANOVA in Table 11, the linear effects of the dye temperature, pH, and concentration were found to be increasingly important for MG dye decolorization. According to the "lack of fit *F* value of 0.715,"the lack of fit was insignificant regarding the pure error. An insignificant lack of fit was regarded as a reliable indicator that the model would be good. The fit of the model was also expressed by the coefficient of regression R^2. The predicted R^2 of immobilized *Mucor* sp. was 0.9837, which is consistent with the adjusted R^2 of 0.967. These findings indicate that the developed model was satisfactory and that the values of the independent factors were accurate with minimal error. The range of the projected response regarding the associated error was measured with adequate precision. A ratio of at least 4 is acceptable; however, a ratio higher than 4 is preferable. The ratio of 24.1 for *Mucor* sp. was high, indicating the reliability of the experimental data. Moreover, according to Table 11, the coefficient of variation (CV%) values for *Mucor* sp. obtained in the study are relatively small, with 2.6. This indicated that the deviations between the experimental and predicted values were low. Figure 20c shows a graph of the Box–Cox diagram of model changes in MG removal (%) using *Mucor* sp. composite determined by a quadratic polynomial. The best lambda value ($\lambda = 1.49$) is between the two red vertical lines, so no data transformation is required. The red line shows

Table 10 Box–Behnken design-based experimental conditions for the decolourization of MG dye by composite *Mucor* sp.

Run	A:pH	B:TP	C:Con	D:Dose	Experimental	Predicted
1	1	0	0	1	70.1	70.38
2	0	0	−1	−1	78	77.06
3	0	0	0	0	90	87.98
4	1	0	1	0	60	59.20
5	1	0	−1	0	73	73.73
6	1	0	0	−1	64	64.15
7	0	1	−1	0	69.26	68.74
8	0	0	1	−1	77	76.85
9	0	0	0	0	90.1	87.98
10	−1	1	0	0	59.1	60.43
11	0	1	0	1	70.03	68.41
12	0	1	1	0	77.7	77.93
13	1	−1	0	0	65	64.92
14	−1	0	1	0	70	69.52
15	−1	0	0	1	64.7	63.05
16	−1	−1	0	0	54.2	55.74
17	0	−1	0	−1	63.78	65.64
18	0	1	0	−1	79.01	79.87
19	1	1	0	0	59.9	59.61
20	−1	0	0	−1	64.9	63.12
21	−1	0	−1	0	54	55.05
22	0	0	1	1	77.92	80.11
23	0	0	0	0	87	87.98
24	0	0	−1	1	78.55	79.96
25	0	−1	0	1	83.86	83.25
26	0	−1	−1	0	80	78.27
27	0	0	0	0	87.8	87.98
28	0	−1	1	0	70	69.02
29	0	0	0	0	85	87.98

the minimum (− 0.2900) and maximum (3.32) values, as well as lambdas at 95% confidence interval value.

Interactive impact of pH on MG dye decolorization

The biosorption of malachite green by the fungus was investigated for a pH range of 5–9. The maximum degree of decolorization (97.8%) was reached at a pH of 7.0, while at a pH of 9, the decolorization rate decreased to 40%. Figure 21a, b shows that the efficacy of dye decolorization using immobilized *Mucor* sp. decreased with rising pH levels. Moreover, Fig. 21c shows that the removal efficiency was 54% at a pH of 5.0 and 30 °C, and it improved to 87.8% at a pH of 7 and 30 °C. Similar findings were made by Alam et al. [70], who discovered that the efficiency of decolorization of malachite green using *Aspergillus niger* was about 97% at a pH of 7.

Interactive impact of temperature on MG dye decolorization

Various environmental factors influenced the degradation of malachite green using *Mucor* sp. This fungal strain degraded malachite green effectively from 303 to 318 °C (Fig. 21c, e, f). Figure 21c, e, f shows that the rate of malachite green decolorization increases as the temperature rises from 25 to 30 °C. Furthermore, malachite green decolorization by *Mucor* sp. ON934589.1 reached a maximum of 91.54% at 303 °C. Conversely, as the temperature rose to 313 °C, the decolorization activity decreased (53%) due to the loss of cell viability or inactivation of the decolorizing enzymes [71]. Arunprasath et al. [2, 72] observed that the optimum temperature (30 °C) was the optimum temperature for the decolorization (92%) of malachite green dye by *Lasiodiplodia* strains.
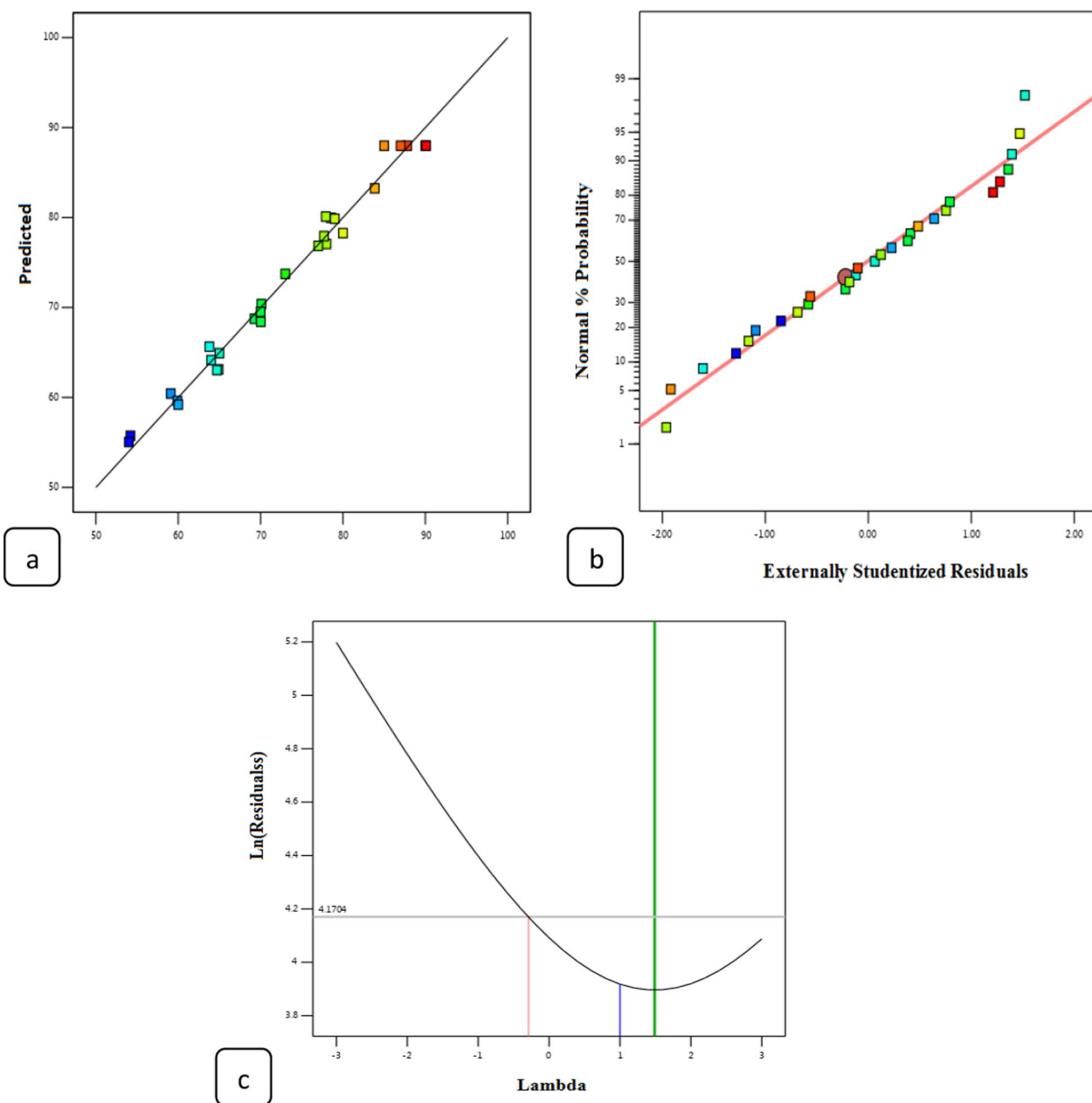
Fig. 20 a Actual and predicted values for the decolourization of MG dye by immobilized *Mucor* sp., **b** normal % probability and **c** Box–Cox plot

Interactive impact of concentration on MG dye decolorization
The adsorption behavior of MG was studied in concentrations of 5–200 mg/L at a pH of 7.0. In addition, 87.7–97.4% of malachite green was eliminated by the immobilized fungus at 5–100 mg/L. The decolorization efficiency of *Mucor* sp. (ON934589.1) fell below 64% when the starting concentration of malachite green approached 150 mg/L. These findings suggest that high concentrations of malachite green impede the

development of *Mucor* sp. (ON934589.1). Figure 21b shows the impact of the initial concentration and contact time on the removal of malachite green dye using immobilized fungus. The immobilized fungus was suppressed at 150 mg/L of malachite green due to the existence of sulfonic acid on the aromatic ring formed in the medium by the increased concentration of malachite green, which inhibited the nucleic acid synthesis and microbial cell proliferation [73]. The findings of this investigation corresponded with those of Ghany et al. [74], who found that

Table 11 Analysis of variance (ANOVA), results for decolourization of MG by immobilized *Mucor* sp.

Source	Sum of squares	df	Mean square	F-value	p-value	
Model	3067.39	14	219.10	60.99	< 0.0001	Significant
A-ph	52.50	1	52.50	14.61	0.0019	
B-Tp	0.2821	1	0.2821	0.0785	0.7834	
C-Con	0.0030	1	0.0030	0.0008	0.9773	
D-Dose	28.43	1	28.43	7.91	0.0138	
AB	25.00	1	25.00	6.96	0.0195	
AC	210.25	1	210.25	58.52	< 0.0001	
AD	9.92	1	9.92	2.76	0.1188	
BC	85.01	1	85.01	23.66	0.0003	
BD	211.12	1	211.12	58.76	< 0.0001	
CD	0.0342	1	0.0342	0.0095	0.9236	
A^2	2210.71	1	2210.71	615.34	< 0.0001	
B^2	566.31	1	566.31	157.63	< 0.0001	
C^2	171.70	1	171.70	47.79	< 0.0001	
D^2	122.32	1	122.32	34.05	< 0.0001	
Residual	50.30	14	3.59			
Lack of fit	31.85	10	3.18	0.6906	0.7115	Not significant
Pure error	18.45	4	4.61			
Cor total	3117.69	28				
SD	1.90				R^2	0.9839
Mean	72.55				Adjusted R^2	0.9677
CV %	2.61				Predicted R^2	0.9319
					Adeq precision	24.1583

Aspergillus fumigates immobilized in polyurethane foam had an optimum malachite green decolorization percentage of about 97.52% (40 mg/L), which reduced to 23% at 70 mg/L.

Impact of contact time on MG dye decolorization

At the optimum dye concentration (50 mg/L) and biosorbent dosage (6 g/L), the impact of contact time on adsorption was examined from 24 to 72 h. Figure 21a, d shows the influence of contact time on the elimination of the MG dye. The range of the MG's adsorption efficiency was 18–72 h, corresponding to 72% and 97%, respectively. Based on the data, 40 h was determined to be the equilibrium time in the sorption process, because no further improvement was observed after reaching maximum adsorption. The high removal efficiency at the beginning of the contact time of 40 h was due to the large surface area available for dye adsorption during the initial stage, and the adsorbent's capacity gradually depleted over time, as the few remaining vacant surface sites became tough to occupy because of repulsive forces between the solute molecules on the solid and bulk phases [75]. Our results correspond with those of Arunprasath et al. [2, 72], who observed that *Lasiodiplodia* sp. could decolorize 81% of malachite green within 36 h.

Biodegradation kinetics: theoretical considerations

The Monod model is used to represent the relationship between the limiting substrate concentration and the specific growth rate using Eqs. (21) and (22).

$$\mu = \frac{\mu \max S}{S + KS} \tag{21}$$

$$\mu = \frac{1}{x} \frac{dx}{dt} \tag{22}$$

Here μ, μmax, and K_s were determined as the biodegradation experiment data. The magnitude of Yx/s was estimated from the slope of the graph of dX dt versus S. The original Monod model becomes inadequate when a substrate prevents biodegradation. Monod derivatives with substrate inhibition adjustment Eqs. (23 and 31), suggested by the Haldane, Aiba–Edward, Luong, Han, and Levenspiel models, have been used to assess the impacts of inhibition at a high substrate concentration and stimulation at a low concentration of substrate [76–79]. Here, S and μ are the substrate concentration and the specific growth rate, respectively; μmax is the maximum specific growth rate; n and m are experimental constants; K_s is the half substrate saturation coefficient, and S_m is
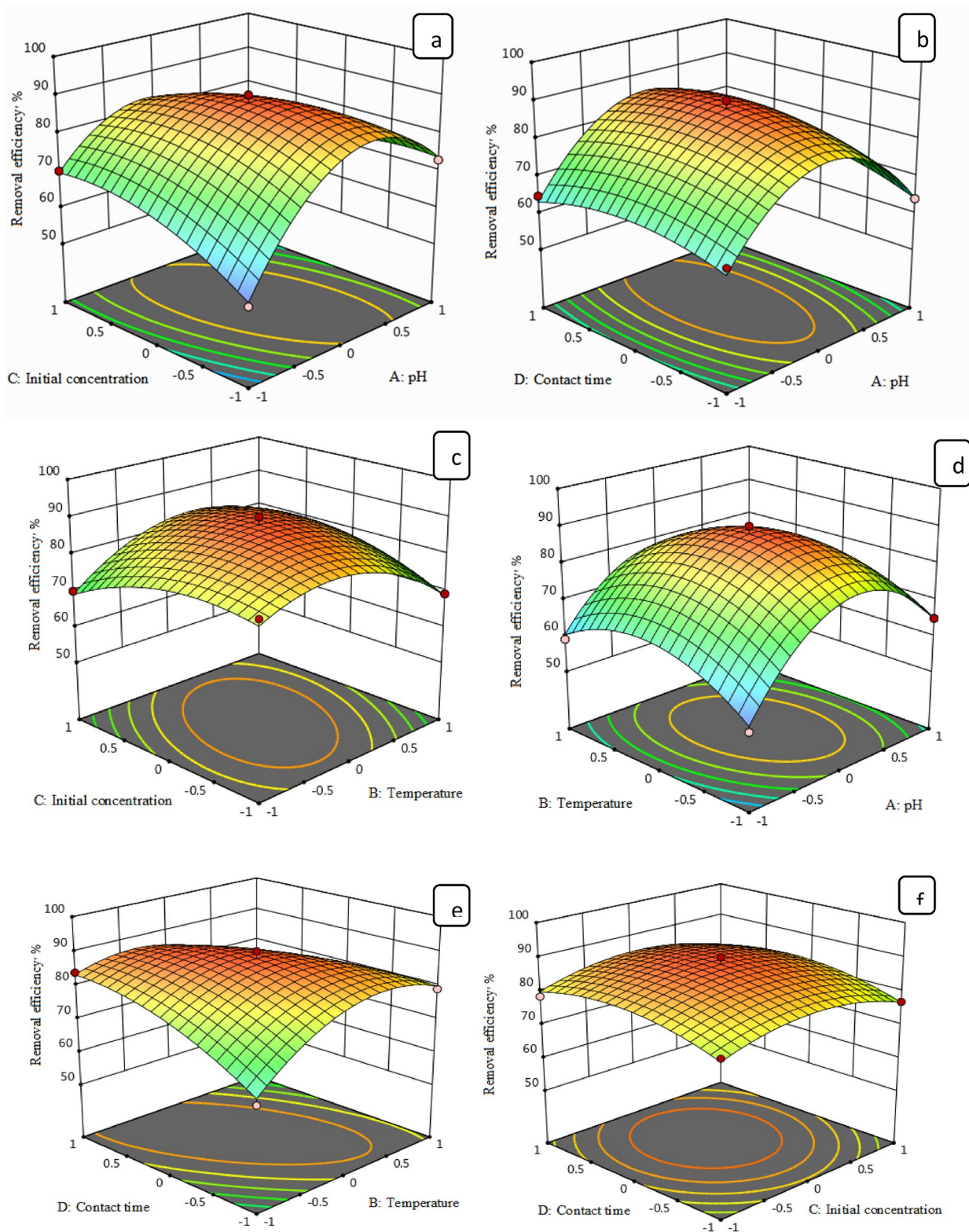
Fig. 21 **a** Cumulative impact of pH and contact time, **b** cumulative impact of pH and MG dye concentration, **c** cumulative impact of pH and temperature, **d** cumulative impact of contact time and MG dye concentration, **e** cumulative impact of contact time and temperature, **f** cumulative impact of temperature and MG dye concentration

the critical inhibitor concentration (mg/L) above which growth ceases.

$$q = \frac{1}{X}\frac{ds}{dt} \tag{23}$$

$$q = \frac{Q \max S}{K2 + S} \tag{24}$$

$$\frac{dy}{dx} = -\frac{q \max SX}{Ks + S} \tag{25}$$

$$\frac{dy}{dx} = -Yx \Big/ s\frac{ds}{dt} \tag{26}$$

$$\mu = Yx \big/ sQ \tag{27}$$

$$\mu = \frac{u \max S}{S + Ks + \left[1 - \frac{s2}{K1}\right]m} \tag{28}$$

$$\mu = \frac{\mu \max S\left[1 - \left(\frac{S}{Sm}\right)\right]n}{(S + KS)} \tag{29}$$

$$\mu = \frac{u \max S1 - \frac{s}{Sm}n}{S + Ks\left[1 - \frac{s}{Sm}\right]m} \tag{30}$$

$$\mu = \frac{\mu \max S \exp(-S/Ki)}{(S + KS)} \tag{31}$$

Here μ = specific growth rate of biomass, μmax = maximum consumption rate constant, S = substrate concentration, $K1$ = the substrate inhibition constant (mg/L), K_s = Monod constant, and S_m = decisive inhibitor concentration (mg/L); n and m are experimental constants.

Biodegradation kinetics of malachite green

For the range of concentrations in the study (5–200 mg L^{-1}), the length of the lag phase t_0 grew exponentially with the malachite green concentration (Fig. 22a). Thus, malachite green was considered to have an inhibiting effect on microbial development at high concentrations. These findings correspond with those
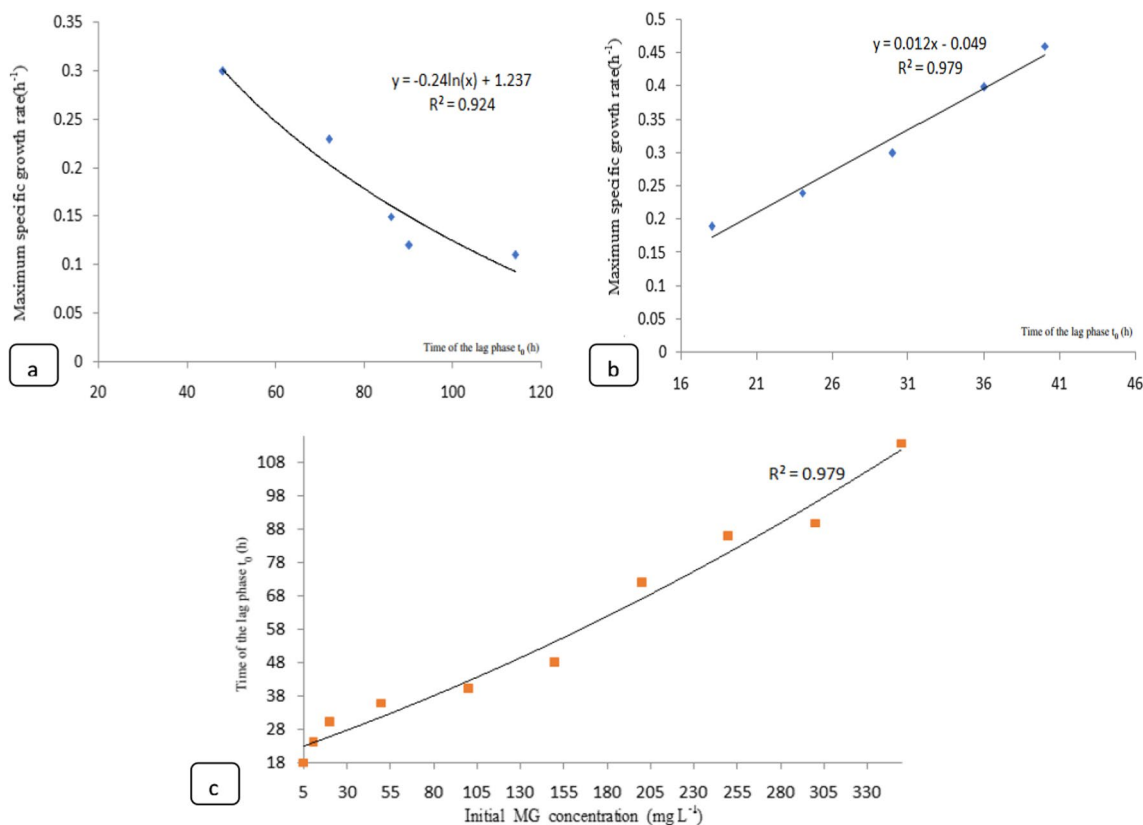

Fig. 22 Time of the lag phase (t_0) versus the initial MG concentration (**a**), and (S_0) Maximum specific growth rate μm versus the time of the lag phase t_0 for S_0 below (**b**), above (**c**) MG concentration mg L^{-1}
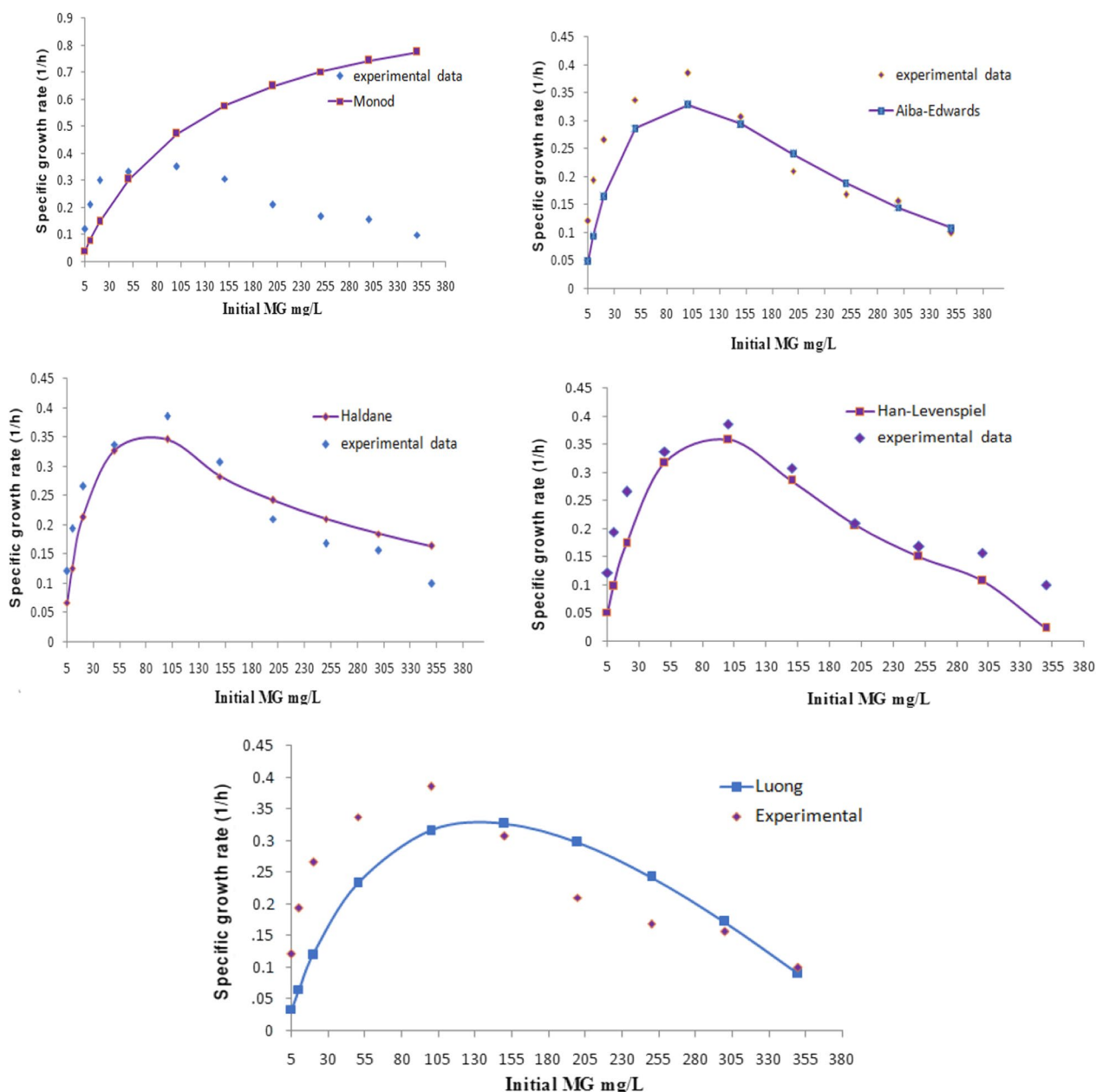
Fig. 23 Experimental and predicted specific substrate consumption rates at different MG concentrations due to different models

previously recorded for mixed cultures [40]. We compared the evolution of the lag phase to the particular growth rate to gain advanced insight into the impact of the lag phase. Two trends were observed, one below (Fig. 22a, c) and one above (Fig. 22b) the 100 mg L^{-1} ^{m}alachite green concentration. The time of the lag phase t_0 rose linearly with an increase in the maximum specific growth rate when the concentration of malachite green (Fig. 22a) was less than 100 mg L^{-1}. However, a contrary trend was observed for concentrations

greater than 100 mg L^{-1} (Fig. 22b), where the length of the lag phase t_0 increased as the maximum specific growth rate decreased. The findings of the curve fitting (Fig. 23) using models such as Monod, Luong, Aiba–Edward, Han, and Levenspiel did not match the experimental results and were excluded. The Luong model provided reasonably acceptable results according to software output and visual examination. The accuracy and statistical analyses of the four kinetic models used in the study revealed that Haldane was

Table 12 Various kinetic models for effect of substrate on growth rate

Models	Equation	μmax (h^{-1})	K_s (mg/L)	K_i	S_m	n	m	RMSE	AICc	AF	R^2
Haldane	$\mu = \dfrac{\mu \max S}{\left(S + KS + \frac{S^2}{Ki}\right)}$	1.02	70	70	–	–	–	0.05	−31.8	0.94	0.961
Han and Levenspiel	$\mu = \dfrac{\mu \max S\left[1-\left(\frac{S}{Sm}\right)\right]n}{(S+KS-)\left[1-\left(\frac{S}{Sm}\right)\right]m}$	1.1	100		360	1	1	0.06	−26.8	0.91	0.922
Luong	$\mu = \dfrac{\mu \max S\left[1-\left(\frac{S}{Sm}\right)\right]n}{(S+KS)}$	1.01	140		400	1		0.09	−20.2	0.88	0.843
Aiba	$\mu = \dfrac{\mu \max S \exp{(-S/Ki)}}{(S+KS)}$	1.6	150	150	–	–	–	0.06	−27.45	0.91	0.822
Monod	$\mu \max = \dfrac{S}{KS}$	0.9	120		–	–	–	0.3	7.5	0.79	0.69

q_{max}: maximal reduction rate (h^{-1}); k_s: half saturation constant for maximal reduction (mg/dm^3); S_m: maximal concentration of substrate tolerated (mg/dm^3); m, n, k: curve parameters; S: substrate concentration (mg/dm^3); RMS: residual mean square

the most accurate model, having the minimum root-mean-square error and AICc values and the maximum adjusted R^2. Table 12 shows the Af and Bf values. The Af and Bf values for Haldane were significant and closest to 1.0. The results of an *F*-test indicated that the Haldane model was better than the Aiba–Edward, Han, Levenspiel, and Luong models, which were 96.1%, 92.2%, 84.43%, and 82.2%, respectively. These results indicate that the Haldane model was superior to the rest. The computed values for the Haldane constants in this work, such as the inhibition constant rate symbolized by the maximal growth rate and half-saturation constant *u*max, *Ks*, and K_i, were 1.02 h^{-1}, 70 mg L^{-1}, and 70 mg L^{-1}.

Microbial toxicity
The results of the microbial toxicity study demonstrated that the medium containing 100 mg/L (control) MG had inhibition zones, indicating the toxicity of MG to the *E. coli* and *Pseudomonas aeruginose* and *Staphylococcus aureus* strains. The treated sample did not demonstrate any growth inhibition when compared to the untreated 100 mg/L MG, showing that the formation of the adsorption process was nontoxic, Fig. 24. This suggests that the effluent might not have any negative effects on its surroundings when released into water bodies.

Reusability of the various adsorbents
The reusability of nano-bentonite and MgO-impregnated clay adsorbents for MG removal was studied. Figure 25 shows the results of recycling studies, and the graph shows that there was a minimal loss in MG removal up to seven cycles. However, after seven cycles, the MG removal effectiveness of the nano-bentonite and MgO-impregnated clay declined from 93–86.85 to 92.2–83%, respectively. Rahimi et al. [80] reported that the reusability of a bentonite/Fe$_3$O$_4$/ZnO nano-composite adsorbent
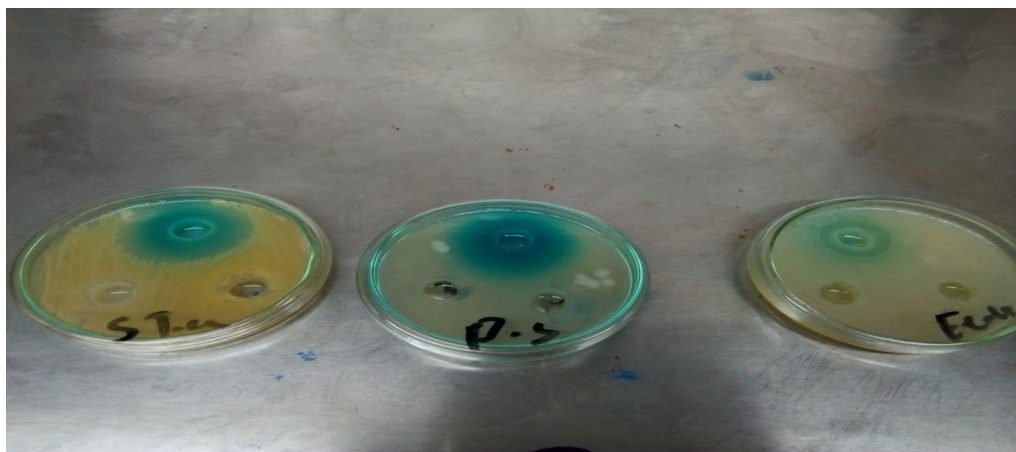

Fig. 24 Microbial toxicity assay showing effect of the untreated and treated dye solution on bacteria
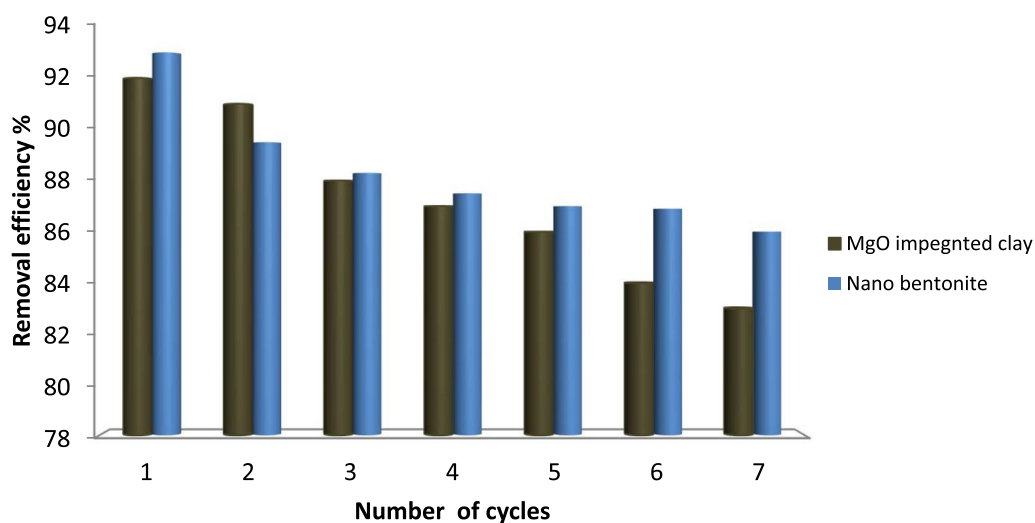
Fig. 25 Percentage removal (%) of the adsorption–desorption cycles of nano-bentonite and MgO impregnated clay

for the removal of methylene blue dye was sustained, even after eight cycles at 86%.

Conclusion

This study has shown that raw bentonite, nano-bentonite, MgO-impregnated clay, and immobilized *Mucor* sp. ON934589.1 are effective adsorbents for removing MG from aqueous solution. The corresponding experimental values of dye adsorption were found to be 0.986%, 0.973%, and 0.983%, which extensively corresponded to the optimal values (0.93%, 0.91%, and 0.931%) predicted by the model RSM for nano-bentonite, MgO-impregnated clay, and *Mucor* sp. (ON934589.1), respectively. The optimal malachite green removal efficiency of MgO-impregnated clay was found at a pH of 9.0, an initial MG concentration of 50 ppm, a dosage of 0.7 g, and a contact time of 60 min. However, the malachite green removal efficiency of nano-clay was observed to be optimal at 35 °C, 7.0pH, 60 min, 1 g/L, and 50 mg/L. The optimal malachite green removal efficiency of raw bentonite was found at a pH of 10.0, an initial MG concentration of 50 ppm, a dosage of 1.2, and a contact time of 60 min. The malachite green adsorption isotherm on MgO-impregnated clay showed maximum consistency with the Freundlich isotherm model, with an R^2 value of 0.982. However, the Langmuir adsorption isotherm was better suited for nano-bentonite ($R^2 = 0.992$) and raw bentonite ($R^2 = 0.952$). The adsorption activities of nano-bentonit, MgO-impregnated clay and raw bentonite were matched to a pseudo-second-order model equation with R^2 values of 0.996 and 0.995, 0.981, respectively. The Gibbs free energy was positive for nano-clay (0.72–7.5 kJ mol^{-1}) and negative for MgO-impregnated clay (-4.07 to -12.9). Moreover, nano-bentonite and MgO-impregnated clay showed enthalpy changes of $-0.151$and 0.196, respectively. A high biodegradation efficiency of 87.8% was obtained during a 72 h decolorization examination of a dye using the isolated fungus *Mucor* sp. (GenBank accession no. ON 934589.1).

Availability of data and materials
All data generated or analyzed during this study are of our own work and it is our pleasure to be available publically. Connect with aurthor-mohamed_taha@nwrc.gov.eg.

Declarations

Ethics approval and consent to participate
Not applicable.

Consent for publication
All authors consent to publishing the manuscript in in Environmental Sciences Europe.

Competing interests
I declare that I have no competing interests.

References

1. Puchongkawarin C, Mattaraj S, Umpuch C (2021) Experimental and modeling studies of methylene blue adsorption onto Na-bentonite clay. Eng Appl Sci Res 48(3):268–279
2. Arunprasath T et al (2019) Biocatalysis and agricultural biotechnology biodegradation of triphenylmethane dye malachite green by a newly isolated fungus strain. Biocatal Agricult Biotechnol 17:672–679
3. Tarekegn MM, Balakrishnan M (2021) Zerovalent iron, nanoclay and iron impregnated. RSC Adv 11(2021):30109–30131
4. Vergis BR et al (2018) Removal of malachite green from aqueous solution by magnetic $CuFe_2O_4$ nano-adsorbent synthesized by one pot solution combustion method. J Nanostruct Chem 8(1):1–12
5. Kabeer FA, John N, Abdulla MH (2019) Biodegradation of malachite green by a newly isolated bacillus *Vietnamensis* sp. MSB17 from continental slope of the Eastern Arabian Sea: enzyme analysis, degradation pathway and toxicity studies. Bioremediat J 23(4):334–342
6. Sutar SS et al (2019) Biocatalysis and agricultural biotechnology biodegradation and detoxi fi cation of malachite green by a newly isolated bioluminescent bacterium photobacterium leiognathi strain MS under RSM optimized culture conditions. Biocatal Agricult Biotechnol 20(May):101183
7. Akpomie KG, Conradie J (2020) Efficient synthesis of magnetic nanoparticle-musa acuminata peel composite for the adsorption of anionic dye. Arab J Chem 13(9):7115–7131. https://doi.org/10.1016/j.arabjc.2020.07.017
8. Akpomie KG, Conradie J (2020b) Efficient synthesis of magnetic nanoparticle-musa acuminata peel composite for the adsorption of anionic dye. Arab J Chem 13:7115–7131
9. Chaturvedi V, Verma P (2015) Biodegradation of malachite green by a novel copper—tolerant ochrobactrum pseudogrignonense strain GGUPV1 isolated from copper mine waste water. Bioresour Bioprocess 2:1–9
10. Ali I (2018) Phytogenic magnetic nanoparticles functionalized. RSC Adv 8:8878–8897
11. Yong Li et al (2015) Photodegradation of malachite green under simulated and natural irradiation: kinetics, products, and pathways. J Hazard Mater 285:127–136
12. Du X Shao F, Wu S (2017) Water quality assessment with hierarchical cluster analysis based on mahalanobis distance. Environ Monit Assess 189:1–12
13. Argumedo-Delira R, Mario JG (2021) Applied sciences trichoderma biomass as an alternative for removal of congo red and malachite green industrial dyes. Appl Sci 11:448
14. Roy DC et al (2020) Isolation and characterization of two bacterial strains from textile effluents having malachite green dye degradation ability. bioRxiv 2020:1–15
15. Shamsizadeh A et al (2014) Tin oxide nanoparticle loaded on activated carbon as new adsorbent for efficient removal of malachite green-oxalate: non-linear kinetics and isotherm study. J Mol Liq 195:212–218
16. Bashanaini SM (2019) Removal of malachite green dye from aqueous solution by adsorption using modified and unmodified local agriculture waste. Sci J Anal Chem 7(2):42
17. Ermias MR, Aklilu G (2017) A comparative study on removal of malachite green dye from waste water using different low cost adsorbents. Water Sci Technol 6(4):262–266
18. Azmier M, Nur A, Afandi S, Solomon O (2017) Optimization of process variables by response surface methodology for malachite green dye removal using lime peel activated carbon. Appl Water Sci 7:717–727
19. Dehmani Y, El Khalki O, Mezougane H (2021) Comparative study on adsorption of cationic dyes and phenol by natural clays. Chem Data Collect 33:100674. https://doi.org/10.1016/j.cdc.2021.100674
20. Dehbi A et al (2019) L P Re of. Biochem Pharmacol. https://doi.org/10.1016/j.jece.2019.103394
21. Ozturk D, Sahan T, Bayram T, Erkus A (2017) Application of response surface methodology (RSM) to optimize the adsorption conditions of cationic basic yellow 2 onto pumice samples as a new adsorbent (RSM)
    to optimize the adsorption conditions of cationic basic yellow 2 onto pumice samples AS. Fresenius Environ Bull 26(May):3285–3292
22. Elkhatib EA, Moharem ML, Saad AF, Attia FA (2022) Using nano-magnesium oxide/bentonite composite for cadmium removal from industrial wastewater. Environ Eng Res 28(2):210545
23. Aichour A, Zaghouane H (2020) Synthesis and characterization of hybrid activated bentonite/alginate composite to improve its effective elimination of dyes stuff from wastewater. Appl Water Sci 10:1–13
24. Al-Asheh S, Banat F (2003) The removal of methylene blue dye from aqueous solutions using activated and non-activated bentonites. Adsorpt Sci Technol 21:451–462
25. Tahir SS, Rauf N (2006) Removal of a cationic dye from aqueous solutions by adsorption onto bentonite clay. Chemosphere 63:1842–1848
26. Abegunde SM, Idowu KS, Adejuwon OM, Adeyemi-Adejolu T (2020) A review on the influence of chemical modification on the performance of adsorbents. Resour Environ Sustain 1(July):100001
27. El-Nagar DA, Massoud SA, Ismail SH (2020) Removal of some heavy metals and fungicides from aqueous solutions using nano-hydroxyapatite, nano-bentonite and nanocomposite. Arab J Chem 13(11):7695–7706. https://doi.org/10.1016/j.arabjc.2020.09.005
28. Messaoudi M et al (2021) Adsorption process of the malachite green onto clay: kinetic and thermodynamic studies. Desalin Water Treat 240(2021):191–202
29. El-Mekkawi SA, Abdelghaffar RA, Abdelghaffar F, Abo El-Enin SA (2021) Application of response surface methodology for color removing from dyeing effluent using de-oiled activated algal biomass. Bull Natl Res Centre 45(1):1. https://doi.org/10.1186/s42269-021-00542-w
30. Gan Li, Zhou F, Owens G, Chen Z (2018) Burkholderia cepacia immobilized on eucalyptus leaves used to simultaneously remove malachite green (MG) and Cr(VI). Colloids Surf B 172(September):526–531. https://doi.org/10.1016/j.colsurfb.2018.09.008
31. Gokulan R, Balaji S, Sivaprakasam P (2021) Optimization of remazol black B removal using biochar produced from caulerpa scalpelliformis using response surface methodology. Adv Mater Sci Eng 2021:1
32. Asnaoui H, Dehmani Y, Khalis M, Hachem E-K (2020) Adsorption of phenol from aqueous solutions by Na—bentonite: kinetic, equilibrium and thermodynamic studies. Int J Environ Anal Chem. https://doi.org/10.1080/03067319.2020.1763328
33. Ahmed MA (2018) Mesoporous MgO nanoparticles as a potential sorbent for removal of fast orange and bromophenol blue dyes mesoporous MgO nanoparticles as a potential sorbent for removal of fast orange and bromophenol blue dyes. Nanotechnol Environ Eng 1:1–11
34. Tabak A et al (2011) Structural analysis of naproxen-intercalated bentonite (Unye). Chem Eng J 174(1):281–288. https://doi.org/10.1016/j.cej.2011.09.027
35. Thakre D et al (2010) Magnesium incorporated bentonite clay for defluoridation of drinking water. J Hazardous Mater 180:122–130
36. Shah I et al (2015) Iron impregnated activated carbon as an efficient adsorbent for the removal of iron impregnated activated carbon as an efficient adsorbent for the removal of methylene blue: regeneration and kinetics studies. PLoS ONE 10(June):e0122603
37. Fabryanty R (2017) Removal of crystal violet dye by adsorption using bentonite–alginate composite. J Environ Chem Eng 5:5677–5687
38. Kowanga KD, Gatebe E, Mauti GO, Mauti EM (2016) Kinetic, sorption isotherms, pseudo-first-order model and pseudo-second-order model studies of Cu(II) and Pb(II) using defatted moringa oleifera seed powder. J Phytopharmacol 5(2):71–78
39. Abdullah NH et al (2021) Enhancing the decolorization of methylene blue using a low-cost super-absorbent aided by response surface methodology. Molecules 26(15):4430
40. Uba G, Abubakar A, Ibrahim S (2021) Optimization of process conditions for effective degradation of azo blue dye by *Streptomyces* sp. DJP15: a secondary modelling approach. Bull Environ Sci 5(2):28–32
41. Sirait M, Manalu PDS (2018) Preparation nature nano-bentonite as adsorbent heavy metal Cd and Hg. J Phys Conf Ser 1120(1):1
42. Ourari A et al (2018) Bentonite modified carbon paste electrode as a selective electrochemical sensor for the detection of cadmium and lead in aqueous solution. Int J Electrochem Sci 13(2):1683–1699
43. Ullah S et al (2021) Adsorption of malachite green dye onto mesoporous natural inorganic clays: their equilibrium isotherm and kinetics studies. Water (Switzerland) 13(7):1

44. Abdelnaby A et al (2022) Application of bentonite clay, date pit, and chitosan nanoparticles as promising adsorbents to sequester toxic lead and cadmium from milk. Biol Trace Elem Res. https://doi.org/10.1007/s12011-022-03353-w

45. Salah BA, Gaber MS, Kandil AHT (2019) The removal of uranium and thorium from their aqueous solutions by 8-hydroxyquinoline immobilized bentonite. Minerals 9(10):1

46. Shan TC, Matar MA, Makky EA, Ali EN (2017) The use of moringa oleifera seed as a natural coagulant for wastewater treatment and heavy metals removal. Appl Water Sci 7(3):1369–1376

47. Akoremale OK, Olaseni SE (2019) Comparative studies on the adsorption of rhodamine B and malachite green from simulated wastewater onto bentonite clay. ChemSearch J 10(2):30–40

48. Blanco-Flores A, Colín-Cruz A, Gutiérrez-Segura E, Vilchis-Nestor A (2016) Removal of malachite green dye from aqueous solution through inexpensive and easily available tuffite, bentonite and vitreous tuff minerals. Rev Latinoamer Recursos Natl 12(1):1–17

49. Zhirong L, Uddin MA, Zhanxue S (2011) FT-IR and XRD analysis of natural Na-bentonite and Cu(II)-loaded Na-bentonite. Spectrochim Acta Part A Mol Biomol Spectrosc 79(5):1013–1016. https://doi.org/10.1016/j.saa.2011.04.013

50. Tastan BE, Özdemir C, Tekinay T (2016) Effects of different culture media on biodegradation of triclosan by rhodotorula mucilaginosa and *Penicillium* sp. Water Sci Technol 74(2):473–481

51. Popli S, Patel UD (2015) Destruction of azo dyes by anaerobic–aerobic sequential biological treatment: a review. Int J Environ Sci Technol 12(1):405–420

52. Hebbar RS et al (2018) Removal of metal ions and humic acids through polyetherimide membrane with grafted bentonite clay. Sci Rep 8(1):1–17. https://doi.org/10.1038/s41598-018-22837-1

53. Chieng HI, Lim LBL, Priyantha N (2015) Enhancing adsorption capacity of toxic malachite green dye through chemically modified breadnut peel: equilibrium, thermodynamics, kinetics and regeneration studies. Environ Technol (UK) 36(1):86–97

54. Jinendra U, Nagabhushana BM, Bilehal D (2021) Comparative adsorptive and kinetic study on the removal of malachite green in aqueous solution using titanium coated graphite and titanium coated graphite with Cnt-Abs nanocomposite. Desalin Water Treat 209:392–401

55. Auta M, Hameed BH (2012) Modified mesoporous clay adsorbent for adsorption isotherm and kinetics of methylene blue. Chem Eng J 198–199:219–227

56. Bao Y, Zhang G (2012) Study of adsorption characteristics of methylene blue onto activated carbon made by salix psammophila. Energy Proc 16(Part B):1141–1146

57. Chauhdary Y et al (2022) Effective removal of reactive and direct dyes from colored wastewater using low-cost novel bentonite nanocomposites. Water (Switzerland) 14(22):1

58. Kuang Y, Zhang X, Zhou S (2020) Adsorption of methylene blue in water onto activated carbon by surfactant modification. Water 12:1–19

59. Mortazavi K et al (2016) Preparation of silver nanoparticle loaded on activated carbon and its application for removal of malachite green from aqueous solution. Synth React Inorgan Met Organ Nanomet Chem 3174(September):1

60. Owolabi RU, Usman MA, Kehinde AJ (2018) Modelling and optimization of process variables for the solution polymerization of styrene using response surface methodology. J King Saud Univ Eng Sci 30(1):22–30

61. Banerjee S, Sharma YC (2013) Equilibrium and kinetic studies for removal of malachite green from aqueous solution by a low cost activated carbon. J Ind Eng Chem 19:1099–1105

62. Abou-Gamra ZM, Ahmed MA (2015) TiO$_2$ nanoparticles for removal of malachite green dye from waste water. Adv Chem Eng Sci 5(July):373–388

63. Ho YS, McKay G (1999) Pseudo-second order model for sorption processes. Process Biochem 34(5):451–465

64. Taher T, Rohendi D, Mohadi R, Lesbani A (2019) Congo red dye removal from aqueous solution by acid-activated bentonite from sarolangun: kinetic, equilibrium, and thermodynamic studies. Arab J Basic Appl Sci 26:5299

65. Muinde VM et al (2017) Adsorption of malachite green from aqueous solutions onto rice husks: kinetic and equilibrium studies. J Environ Prot 08:215–230

66. Zhang Z, Hara IMO, Kent GA, Doherty WOS (2013) Comparative study on adsorption of two cationic dyes by milled sugarcane bagasse. Ind Crops Prod 42:41–49

67. Belbachir I, Makhoukhi B (2017) Adsorption of bezathren dyes onto sodic bentonite from aqueous solutions. J Taiwan Inst Chem Eng 75:105–111

68. Gündüz F, Bayrak B (2017) Biosorption of malachite green from an aqueous solution using pomegranate peel: equilibrium modelling, kinetic and thermodynamic studies. J Mol Liq 243:790–798

69. Archana S et al (2022) Numerical investigations of response surface methodology for organic dye adsorption onto Mg–Al LDH–GO nano hybrid: an optimization, kinetics and isothermal studies. J Indian Chem Soc 99(1):100249. https://doi.org/10.1016/j.jics.2021.100249

70. Zahangir AM, Khan MJH, Kabbashi NA, Abu Sayem SM (2018) Development of an effective biosorbent by fungal immobilization technique for removal of dyes. Waste Biomass Valoriz 9(4):681–690

71. Afrin S et al (2021) The degradation of textile industry dyes using the effective bacterial consortium. Heliyon 7(10):e08102. https://doi.org/10.1016/j.heliyon.2021.e08102

72. Arunprasath T (2019) Biocatalysis and agricultural biotechnology biodegradation of triphenylmethane dye malachite green by a newly isolated fungus strain. Biocatal Agricult Biotechnol 17:672–679

73. Barapatre A, Aadil KR, Jha H (2017) Biodegradation of malachite green by the ligninolytic fungus aspergillus flavus. Clean: Soil, Air, Water 45(4):1–12

74. Ghany T, Abboud M, Alawlaqi M, Shater A (2019) Dead biomass of thermophilic aspergillus fumigatus for congo red biosorption. Egypt J Exp Biol (Bot) 15(1):1

75. Kumar PS, Sivaprakash S, Jayakumar N (2017) Removal of methylene blue dye from aqueous solutions using lagerstroemia indica seed (LIS) activated carbon. Int J Mater Sci 12(1):107–116. http://www.ripublication.com

76. Basu S, Dasgupta M, Chakraborty B (2014) Removal of chromium(VI) by bacillus subtilis isolated from East Calcutta Wetlands, West Bengal, India. Int J Biosci Biochem Bioinform 4(1):7–10

77. Hamitouche AE et al (2012) Relevance of the luong model to describe the biodegradation of phenol by mixed culture in a batch reactor. Ann Microbiol 62(2):581–586

78. Johari MS (2014) Mathematical modeling of the growth kinetics of *Bacillus* sp. on tannery effluent containing chromate. J Environ Bioremed Toxicol 2(1):6–10

79. Han* K, Levenspie O (1988) Extended monod kinetics for substrate, product, and cell inhibition. Biotechnol Bioeng 32:430–447

80. Rahimi SM, Panahi AH, Allahyari E, Nasseh N (2022) Breaking down of low-biodegradation Acid Red 206 dye using bentonite/Fe3O4/ZnO magnetic nanocomposite as a novel photo-catalyst in presence of UV light. Chem Phys Lett 794:139480

81. Garg VK, Kumar R, Gupta R (2004) Removal of malachite green dye from aqueous solution by adsorption using agro-industry waste: a case study of prosopis cineraria. Dyes Pigm 62(1):1–10

82. Chowdhury S, Saha P (2010) Sea shell powder as a new adsorbent to remove basic green 4 (malachite green) from aqueous solutions: equilibrium, kinetic and thermodynamic studies. Chem Eng J 164:168–177. https://doi.org/10.1016/j.cej.2010.08.050

83. Geetha P, Latha M, Koshy M (2015) Biosorption of malachite green dye from aqueous solution by calcium alginate nanoparticles: equilibrium study. J Mol Liq 212:723–730. https://doi.org/10.1016/j.molliq.2015.10.035

84. Mohammadi A, Daemi H, Barikani M (2014) Fast removal of malachite green dye using novel superparamagnetic sodium alginate-coated Fe3O4 nanoparticles. Int J Biol Macromol 69:447–455. https://doi.org/10.1016/j.ijbiomac.2014.05.042

85. Sundararaman TR et al (2021) Adsorptive removal of malachite green dye onto coal-associated soil and conditions optimization. Int J Biol Macromol 2021:1–11

86. El-Zahhar AA, Awwad NS (2016) Removal of malachite green dye from aqueous solutions using organically modified hydroxyapatite. J Environ Chem Eng 4:633–638. https://doi.org/10.1016/j.jece.2015.12.014

Publisher's Note